Cerebral Cortex, January 2016;26: 346–357

doi: 10.1093/cercor/bhu260
Advance Access Publication Date: 10 November 2014
Original Article

ORIGINAL ARTICLE

Oxygen Level and LFP in Task-Positive and Task-Negative Areas: Bridging BOLD fMRI and Electrophysiology

William J. Bentley[1], Jingfeng M. Li[1], Abraham Z. Snyder[2,3], Marcus E. Raichle[1,2,3], and Lawrence H. Snyder[1]

[1]Department of Anatomy and Neurobiology, Washington University School of Medicine, St. Louis, MO 63110, USA, [2]Department of Radiology, and [3]Department of Neurology, Washington University School of Medicine, St. Louis, MO 63110, USA

Address correspondence to Jingfeng M. Li, Department of Anatomy and Neurobiology, Washington University School of Medicine, 660 S Euclid Ave., Box 8108, St. Louis, MO 63110, USA. Email: jing@eye-hand.wustl.edu

W.J.B. and J.M.L. contributed equally to this study.

Abstract

The human default mode network (DMN) shows decreased blood oxygen level dependent (BOLD) signals in response to a wide range of attention-demanding tasks. Our understanding of the specifics regarding the neural activity underlying these "task-negative" BOLD responses remains incomplete. We paired oxygen polarography, an electrode-based oxygen measurement technique, with standard electrophysiological recording to assess the relationship of oxygen and neural activity in task-negative posterior cingulate cortex (PCC), a hub of the DMN, and visually responsive task-positive area V3 in the awake macaque. In response to engaging visual stimulation, oxygen, LFP power, and multi-unit activity in PCC showed transient activation followed by sustained suppression. In V3, oxygen, LFP power, and multi-unit activity showed an initial phasic response to the stimulus followed by sustained activation. Oxygen responses were correlated with LFP power in both areas, although the apparent hemodynamic coupling between oxygen level and electrophysiology differed across areas. Our results suggest that oxygen responses reflect changes in LFP power and multi-unit activity and that either the coupling of neural activity to blood flow and metabolism differs between PCC and V3 or computing a linear transformation from a single LFP band to oxygen level does not capture the true physiological process.

Key words: default mode network, neurohemodynamic coupling, oxygen polarography, power spectrum, transfer function

Introduction

The default mode network (DMN) was first identified through human brain imaging as a set of regions in which blood flow decreases, relative to baseline, in response to a wide range of novel, attention-demanding tasks and stimuli (Shulman, Fiez, et al. 1997; Binder et al. 1999; Mazoyer et al. 2001; Raichle et al. 2001). These "task-negative" regions, which include the anterior and posterior cingulate cortices, medial and lateral parietal cortices, and medial prefrontal cortex, are collectively considered to be a network because they show correlated intrinsic blood oxygen level dependent (BOLD) fluctuations even when subjects are at rest (Raichle et al. 2001). The human DMN is believed to instantiate high-order cognitive functions, such as self-referential thinking, social cognition, and episodic recall (Buckner et al. 2008). Altered BOLD fMRI activity in the DMN has been linked to neurological and psychiatric disorders, such as schizophrenia and depression (Anticevic et al. 2012). Yet, substantial gaps exist in the

understanding of how BOLD is related to the underlying neural activity in the DMN. We address this issue in the current study.

The macaque brain includes a network that is homologous to the human DMN. As in humans, the macaque DMN exhibits spontaneously correlated intrinsic activity in the absence of task performance (Greicius et al. 2003; Fox et al. 2005; Vincent et al. 2007; Mantini et al. 2011). These regions also exhibit task-negative responses in a variety of behavioral paradigms (Kojima et al. 2009; Mantini et al. 2011). However, these task-negative responses have appeared to be less reliable than those in humans. In humans, task-negative responses in the DMN are a robust finding in many PET and fMRI studies. In monkeys, task-negative responses in PET differ substantially across animals and tasks (Kojima et al. 2009), and task-negative responses in fMRI have been reported only in a meta-analysis that combines data from 8 individual studies and 15 experiments (Mantini et al. 2011); none of the individual studies reported task-negative effects. The difficulty of observing task-negative responses in macaques compared with humans could reflect a species difference, perhaps related to differences in how the DMN is used in the two species (Mantini et al. 2013). Alternatively, however, the difference may reflect the fact that animals are extensively trained and reinforced to hold still and fixate during fMRI data collection. As a result, animals may never fully disengage with the environment and may never fully engage their DMN.

Although it is generally accepted that BOLD signals reflect neural activity ([Logothetis et al. 2001; Thompson 2005; Shmuel et al. 2006; Devor et al. 2007; Lu et al. 2007; Goense and Logothetis 2008; He et al. 2008; Maier et al. 2008; Ekstrom et al. 2009; Foster et al. 2012; Magri et al. 2012; Ramot et al. 2012; Pan et al. 2013] reviewed by [Singh 2012]), gaps remain in our understanding of the specific neural activity that underlies task-induced fMRI responses. Simultaneous BOLD fMRI in combination with electrophysiology requires highly specialized equipment unavailable to most (Logothetis et al. 2001). Studies in monkeys and rodents that have compared BOLD fMRI and high-resolution invasive electrophysiology have focused on primary visual and somatosensory cortex, that is, "task-positive" brain areas that show increased activity in response to particular stimuli or tasks; moreover, most of these studies have been done in anesthetized animals (Logothetis et al. 2001; Kayser 2004; Niessing 2005; Shmuel et al. 2006; Devor et al. 2007). As far as we are aware, simultaneous fMRI electrophysiology has not been performed in any node of the DMN. Two studies in macaques and a handful in humans have recorded electrophysiology in the DMN, but the findings were not directly linked back to BOLD fMRI (Hayden et al. 2009; Jerbi 2010; Dastjerdi et al. 2011; Ossandon et al. 2011; Foster and Parvizi 2012; Ramot et al. 2012; Gabbott and Rolls 2013). Direct comparison of BOLD fMRI and invasive electrophysiological task-negative responses obtained from identical locations under identical task conditions has not been done.

To directly compare task-negative BOLD responses in macaques to the underlying neural activity, we used oxygen polarography as a surrogate for BOLD fMRI. Oxygen polarography is an electrode-based technique for measuring tissue oxygen that can be readily combined with standard macaque electrophysiology. The spatial specificity and temporal resolution of our oxygen polarographic system far exceed those of fMRI and are comparable with the scale of the electrophysiology. We used this system to record oxygen level and local field potentials (LFPs) in posterior cingulate cortex (PCC), a hub of the DMN (van den Heuvel and Sporns 2013), and in task-positive area V3. Monkeys sat in a quiet, dark room with minimal restrictions and naturally entered a "resting" state during the long (30 s) inter-trial intervals. Every 45 s, they were engaged by 15 s of whole-field visual stimulation. This stimulus drove increases in both oxygen level and LFP power within V3. In PCC, stimulation produced a transient increase followed by a sustained decrease in both measures. Oxygen and LFP responses were clearly related across a wide range of LFP frequencies in both regions. However, the specifics of LFP–oxygen relationship differed between the two regions.

Materials and Methods

Oxygen Recording

Oxygen polarography was introduced to neuroscience in the mid-twentieth century but went out of favor long ago (Bronk et al. 1946). It has recently been reintroduced and has been used to study oxygen changes in sensory areas and the cerebellum (Thompson et al. 2004; Masamoto et al. 2008; Thomsen et al. 2009; Lowry et al. 2010). Polarography is an electrochemical technique. When the voltage of a noble metal cathode is held at around −0.8 V relative to a reference electrode, the primary half-cell reaction is reduction of oxygen. The reaction rate is limited by oxygen concentration, and thus, the current required to maintain the polarization is proportional to oxygen concentration (Clark et al. 1953; Fatt 1976).

We utilized specialized platinum microelectrodes suitable for both oxygen polarographic redox control and electrophysiologic recording (FHC instruments) as a cathode. An Ag/AgCl reference electrode (Grass Technologies) was placed on the back of the head at a location with minimal underlying musculature and no response to body or limb movements. The skin was lightly abraded to minimize sweat and movement potentials, and a layer of Ten20 EEG paste was applied. A commercial voltage clamp (Unisense PA2000) provided a measure of the clamping current. Our system allowed simultaneous oxygen recording at four sites with a temporal resolution from 0 to 20 Hz and a spatial specificity of 30–100 μm (Fatt 1976). We could then record LFP and multi-unit activity from these same electrodes by disconnecting them from the voltage clamp and connecting them to standard electrophysiologic amplifiers.

Animals, Behavior, and Stimulus

Two macaques served as subjects in this study. Animals were cared for and handled in accordance with the *Guide for the Care and Use of Laboratory Animals*, and all procedures were approved by the Washington University Animal Studies Committee. During recording, macaques were fully hydrated and sat head-fixed in a dark room facing a wide-field textured screen. Behavior was unconstrained, and the animals had no expectation of a task or reward. Every 45 s, 15 s of dim 1 Hz stroboscopic illumination with a 0.5 s duty cycle was presented. Illumination filled ~45° of visual angle directly in front of the animal and contained low-frequency spatial contours (blurred shadows) due to the projector. This blurring is visually equivalent to applying a 2-pixel radius Gaussian filter to a 259- by 194- pixel image (e.g., Supplementary Fig. 1). Each 15 s stimulus period and subsequent 30 s rest period was considered one trial. On one-eighth of trials, an auditory tone was sounded at the onset of the visual stimulus. Responses on trials with and without tones were similar and so were pooled in the analysis (below).

Animals naturally relaxed in between stimulus presentations. During the interstimulus period, the velocity of spontaneous eye movements typically slowed and the eyelids often partially or fully closed (37% of the time, monitored using an ISCAN camera

and software [ETL-400]). With each onset of the visual stimulus, even though there was no explicit task, animals opened their eyes and made high-velocity saccades toward the stimulus. Thus, each trial contained two distinct states: aroused and engagement with an external stimulus and unstimulated "resting" interstimulus periods in which animals appeared disengaged from the external world and drowsy.

Recording

The brain was accessed via bilateral 15-mm (internal diameter) chronic custom recording chambers custom-manufactured from Delrin and stabilized using a poly methyl methacrylate headcap affixed to the skull with ceramic screws (Thomas Recording GmbH). T1-weighted MRI images (MPRAGE; 0.5-mm isotropic voxels) were obtained using a custom phantom in the chamber that provides visualization of the chamber and allows for the virtual projection of a chamber-based coordinate system down into the brain. Two small manganese injections were placed in each monkey to determine the alignment of our chamber coordinates with the brain anatomy (Supplementary Fig. 2A). Prior to data collection, we used MRI images from each animal and standard atlas definitions (Saleem and Logothetis 2007) to target PCC and V3 in the left and right hemispheres (Supplementary Fig. 2B). We then recorded local field potentials (LFPs) and multi-unit activity in and around the targeted areas, refining the boundaries based on the extent of negative and positive electrophysiological responses to visual stimuli in PCC and V3, respectively. During data collection, for each recording session, 4 specialized platinum microelectrodes were inserted into left and right PCC and V3 with a multi-electrode micro-drive (NAN Instruments, Inc.). Placement in gray matter was confirmed by multi-unit activity. Electrodes were referenced to a metal guide tube that traversed the soft tissue outside the brain and just penetrated the dura.

We recorded from 23 and 21 sites in PCC and V3, respectively. Oxygen and LFP were recorded serially. At each site, 15–40 trials (45-s cycles of alternating stimulation and quiet rest in the dark) of LFP were collected. Next, we polarized the electrodes (see above), waited 30 min to ensure electrochemical stability, and then collected 45 trials of oxygen data at each site. In total, data were obtained from 1025 and 942 trials for oxygen, and 605 trials and 607 trials for LFP, in PCC and V3, respectively. Oxygen was low-pass-filtered at 20 Hz, LFP was low-pass-filtered at 300 Hz, and both were sampled and stored at 1 kHz using the Plexon MAP system (Plexon, Inc.).

Analysis

Oxygen polarographic signals, like BOLD signals, reflect relative rather than absolute oxygen levels. The polarographic current values were therefore, like fMRI BOLD data, expressed as percentage deviation from baseline. Baseline was defined as mean of the last 5 s of all trials. LFP data were converted to the frequency domain using the continuous wavelet transform. The mother wavelet used was a complex Morlet wavelet:

$$\text{Complex Morlet}\ (x) = \left(\frac{1}{\sqrt{2\pi}}\right) \times e^{(i2\pi x)} \times e^{-(x^2/2)}$$

Supplementary Figure 3 shows that the temporal smoothing of this method is proportional to the period of the estimated frequency, with more temporal smoothing for lower frequencies. Similar to oxygen, the power in each frequency band was expressed as percent deviation from the power in that band during baseline. Oxygen and LFP signals were then averaged across trials, recording sites, and monkeys. Prior to averaging, each trial's response was offset by the mean of the last 5 s of the previous and current trial. This removes low-frequency effects such as linear trends that effect response variance but has no effect on the mean response.

In order to compare the relationship between oxygen and neural activity, we assessed the lagged cross-correlation between oxygen and LFP. For statistical analysis, the bounded distribution of Pearson's r values was shifted to a normal distribution using Fisher's z transform. For the analysis illustrated in Figure 5, Rows 1 through 4, standard hemodynamic response functions (HRFs) (the sum of two gamma functions) were generated using the SPM5 fMRI Matlab toolbox (http://www.fil.ion.ucl.ac.uk/spm/software/spm5/) and to fit the data: a canonical HRF based on empirical data from visual stimulation in humans, with a single free-scale parameter (Worsley and Friston 1995), and a generic HRF with all 8 parameters of the two gamma functions free. These functions have previously been used to relate LFP and hemodynamic signals (Rosa et al. 2010; Wu et al. 2010). Free parameters were fit by minimizing the squared deviation of the predicted and observed oxygen responses.

To provide a model-free approach to assessing the relationship between oxygen and LFP power, transfer functions were computed using linear systems theory. The fast Fourier transform (FFT) of the oxygen signal was divided by the FFT of the LFP signal, and the result was inverse Fourier transformed. This process derives a mathematically exact convolution kernel that converts the LFP signal to the estimated oxygen signal (Fig. 5, Rows 5 and 6). However, assumptions inherent to the FFT lead to over-fitting in frequency domain of real world signals, which can lead to artificial zeroes in the FFT. When zeroes occur in the FFT of the denominator (FFT(LFP)), they result in artificially inflated frequencies in the transfer function that obscure visualization of its primary behavior. To reduce the impact of over-fitting, we multiplied each signal by 25% Gaussian white noise prior to computing the FFT, which regularizes the frequency domain representation of the modeled signal by reducing artificial zeroes. To remove effects of the white noise on the estimated kernel, we repeated this process 500 times and took the mean result. To further focus on the primary features of the kernel, we then low-pass-filtered the transform at 0.27 Hz (Press et al. 2007).

Results

To investigate the relationship between BOLD responses and neural activity, we recorded local oxygen level and LFP serially from V3 and PCC of two macaque monkeys at rest and engaged by a visual stimulus. V3 is a visually responsive "task-positive" brain region. PCC is a "task-negative" brain region expected to decrease activity during task engagement (Mantini et al. 2011). Visual stimulation consisted of 15–45 repetitions of 15 s of 1-Hz stroboscopic low-spatial-frequency patterned illumination. Each stimulus was followed by 30 s of darkness to allow the macaque to return to a baseline (unstimulated) resting state. Animals were head-fixed and seated in a primate chair but were otherwise unrestrained. No rewards were delivered. Visual monitoring and eye tracking under infrared illumination confirmed that they were engaged with the stimulus when it was presented and otherwise were relaxed and drowsy, partially or fully closing their eyes 37% of the time. The basic results described in the paper were similar for the two monkeys, and they were combined.

Visual stimulation resulted in an increase in mean oxygen level averaged over the stimulus response compared to baseline of 0.77 ± 0.08% in V3 and −1.82 ± 0.21% in PCC ($P < 0.0001$). The results in the two monkeys were similar to each other (in V3, $F_{1,20} = 0.62$, $P = 0.4$; in PCC, $F_{1,22} = 1.13$, $P = 0.3$). In V3, the oxygen level increased after a short delay, peaking at 2.0% above baseline 6.2 s after stimulus onset. Oxygen then decreased to a sustained level of 0.3% above baseline during stimulation. A second peak of 0.7% occurred 3.2 s after the final flash, followed by 9.4 s of values below baseline. In PCC, there was an initial positive response that was indistinguishable for the first 3.1 s from the initial positive response in V3. The initial PCC response peaked at 1.1%, 3.7 s after stimulus onset. PCC oxygen then decreased sharply, falling to −2.5% below baseline at 11.7 s and remained negative for 15.4 s after the end of stimulation (Fig. 1). Oxygen responses were similar in the two monkeys (Supplementary Fig. 4). These results, obtained from oxygen polarographic measurements in monkeys, are similar to the results obtained from BOLD measurements in humans under similar circumstances (Kwong et al. 1992; Ogawa et al. 1992; Lustig et al. 2003).

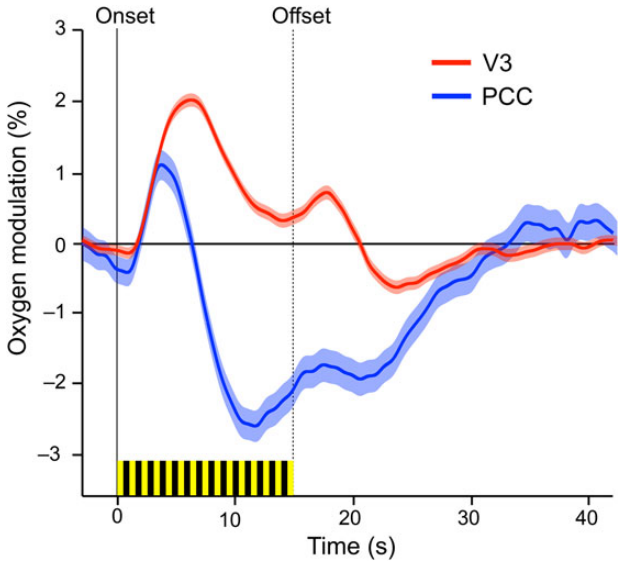

Figure 1. Percent oxygen modulation (mean ± SEM) relative to the period 0–5 s before stimulus onset. Yellow-black bars mark the 15-s, 1-Hz stroboscopic stimulus. Both areas show a 2.3-s delay followed by an increase in oxygen, peaking at 3.7 s in PCC and 6.2 s in V3. This is followed by a sustained positive response in V3 and a sustained negative response in PCC. After the stimulus is turned off, there is a late suppression in both areas followed by a return to baseline at ~15 s after the end of stimulation. Data from 1025 and 942 trials are included in the PCC and V3 traces, respectively.

Changes in oxygen level lagged but otherwise qualitatively tracked the stimulus-evoked changes in LFP power recorded from the same electrodes used for polarography. Figure 2*a* shows that, like oxygen, LFP power increased in V3 and decreased in PCC during stimulation overall. Increases in power greater than 2 standard errors above baseline are shown in yellow and red, and decreases are shown in blue. Figure 2*b* shows the mean (±SEM) change in LFP power as a function of frequency during the period 5–15 s after the onset of visual stimulation relative to the subsequent 30 s of darkness. Supplementary Figure 6 shows the LFP power during the visual stimulation and the subsequent 30 s of darkness. The LFP power change was similar in the two monkeys at most frequencies, except 8–32 Hz in V3, where there was a trend toward weaker modulation in Monkey 1 compared with Monkey 2 (Supplementary Fig. 7 and *P*-values in Supplementary Fig. 5). In V3, LFP power is significantly increased at frequencies of >16 Hz and significantly decreased from 4 to 16 Hz. A similar pattern has been reported in other monkey electrophysiology studies, for example Bartolo et al. (2011). In contrast, LFP power in PCC was suppressed across the entire frequency range (1–150 Hz), with the magnitude of the suppression varying by frequency.

LFP power modulation showed many temporal and spectral features that were not visible in the oxygen response. To examine these responses in detail, we collapsed the LFP response into near-logarithmic bands that approximate the common EEG frequency ranges (Fig. 3): delta: 1–4 Hz, theta: 4–8 Hz, alpha: 8–16 Hz, beta: 16–32 Hz, low gamma: 32–64, and high gamma: 64–150 Hz. We did not find well-separated rhythms with distinct dynamics corresponding to common EEG frequency ranges (Supplementary Fig. 6 and Fig. 2*b*). Instead, the LFP response patterns changed slowly with frequency, so that the precise boundaries of these bands had only minor effects on the results.

Across all bands in both V3 and PCC, there was an increase in LFP power at stimulus onset. Onset response magnitude was roughly similar in the two regions. Following the onset response, the LFP responses markedly differed. We separated the LFP responses into tonic modulation and phasic responses to each flash. Tonic LFP power modulation was evaluated as the mean power during the inter-flash intervals (100 ms prior to each

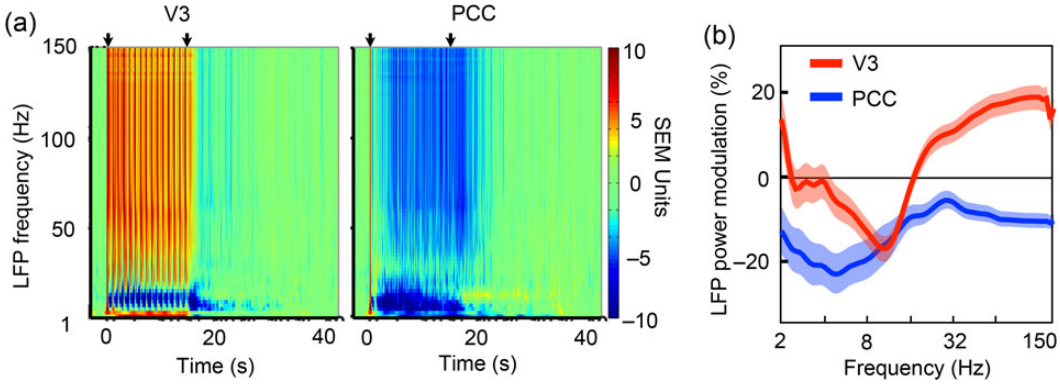

Figure 2. (*a*) LFP power modulation relative to baseline (0–5 s before stimulus onset) in standard error units (SEM is estimated based on baseline activity). Arrows indicate stimulus onset and offset. Data from 607 and 605 trials are included for V3 (left) and PCC (right), respectively. (*b*) LFP power modulation (mean ± SEM) as a function of frequency (log) during stimulation for V3 and PCC.

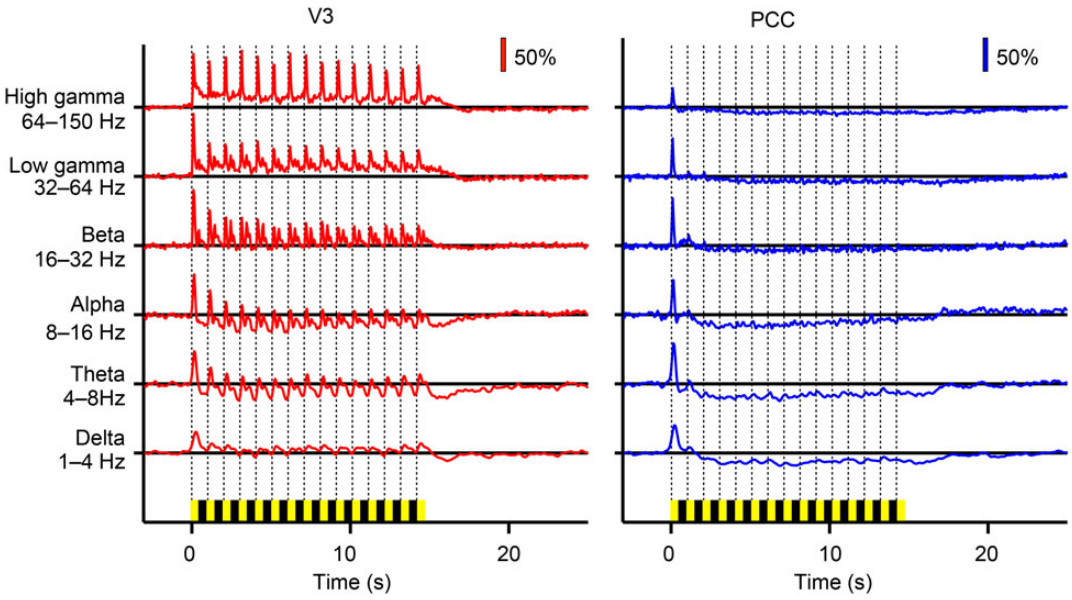

Figure 3. Percent modulation of LFP power for standard EEG bands. V3 shows complex phasic responses riding on top of tonic increases (gamma and delta) and decreases (alpha and theta) in power relative to baseline. PCC shows smaller phasic responses and tonic decreases.

flash, averaged over the stimulation period) relative to the power in the inter-trial interval. In V3, the tonic power was elevated in gamma and delta (both $P < 0.0001$, suppressed in theta and alpha (both $P < 0.0001$), and weakly though significantly suppressed in beta ($P < 0.0001$). As noted in the Materials and Methods section, the method used to estimate the power also smooths (low-pass filters) the data. This effect is largely negligible in the time scale we are interested in, except for delta band, where the smoothing has a full-width half-height of 900 ms (Supplementary Fig. 3). Thus, the fact that power in the delta band shows a tonic increase could be an artifact of the combination of a phasic increase with each flash, plus temporal smoothing, rather than a true activation of delta band frequencies that is sustained across the inter-flash intervals. Differentiating these two possibilities is beyond the scope of this study. In PCC, all bands showed tonic suppression (all $P < 0.0001$).

How long it took to reach the tonic level of LFP power, and how long the tonic level was sustained after the end of the stimulus, varied across frequency bands (Fig. 3). In V3, tonic increases in power in the gamma, and delta bands occurred immediately following stimulus onset. Gamma power was maintained at a constant level for 0.7 s after the end of stimulation before falling to baseline, whereas delta power dropped almost immediately to a pronounced post-stimulation undershoot. Tonic decreases in V3 power (alpha and theta bands) showed much slower dynamics, evolving over the first several flashes and remaining depressed for 1.8 s before returning to baseline. In PCC, tonic suppression developed and decayed slowly in all bands, reaching its peak after several seconds and returning to baseline ~8 s after the last flash. As in V3, tonic LFP dynamics in PCC varied with frequency. The time to peak tonic suppression depended on the frequency band (analysis of variance, $F_{5,3624} = 4.31$, $P < 0.001$). The slowest development of tonic suppression was in the beta and low-gamma range.

Phasic responses to each cycle of the flashing stimulus were superimposed on the tonic LFP power modulations. We were particularly interested in the phasic responses at steady state and so averaged the LFP responses to the fourth through fifteenth flashes in each area (Fig. 4). The flash-triggered average was aligned so that the mean power in the interval 100 ms prior to each flash was set to zero. There was an abrupt increase in power at the onset of each flash, with additional ripples just before and after flash offset. Phasic responses were present at all frequencies in both regions; however, they were ~10 times larger in V3 than in PCC. The strongest phasic responses occurred at higher frequencies in V3 compared with PCC (high gamma versus beta, respectively). In addition to phasic responses in LFP power, the raw LFP also showed consistent visually evoked changes in both V3 and PCC. Each cycle of the stimulus evoked a response, and these responses were similar across time, that is, the potential evoked by the first flash was similar to the potential evoked by each of the later flashes (Supplementary Fig. 8A). Removing the mean-evoked potential has minimum effect on LFP power responses, suggesting that neither tonic nor phasic responses result from the evoked potentials (Supplementary Fig. 8B).

Oxygen responses did not match the phasic responses in LFP power or evoked potentials, but they did roughly match tonic LFP responses. Oxygen level increased in V3 and decreased in PCC (Fig. 1). Phasic LFP responses were positive in both regions and showed complex patterns that were not directly reflected in the oxygen signal. In contrast, the tonic LFP responses behaved similar to oxygen level, generally rising in V3 and falling in PCC. Note that both oxygen and LFP power showed an initial positive response in PCC that was sustained for longer than the phasic flash responses.

Next, we quantitatively evaluated the relationship between oxygen level and LFP power in each area. Prior studies suggested that hemodynamic responses are most consistently correlated with gamma-band LFP (Singh 2012). To test this relationship, we computed the linear correlation between trial-averaged oxygen and trial-averaged gamma-band LFP power responses. Since fMRI BOLD and our own recordings suggest that oxygen responses are lagged compared with neuronal activity, we computed the cross-correlation at lags from −7 to +12 s. Gamma-band power was highly correlated with oxygen in both V3 and

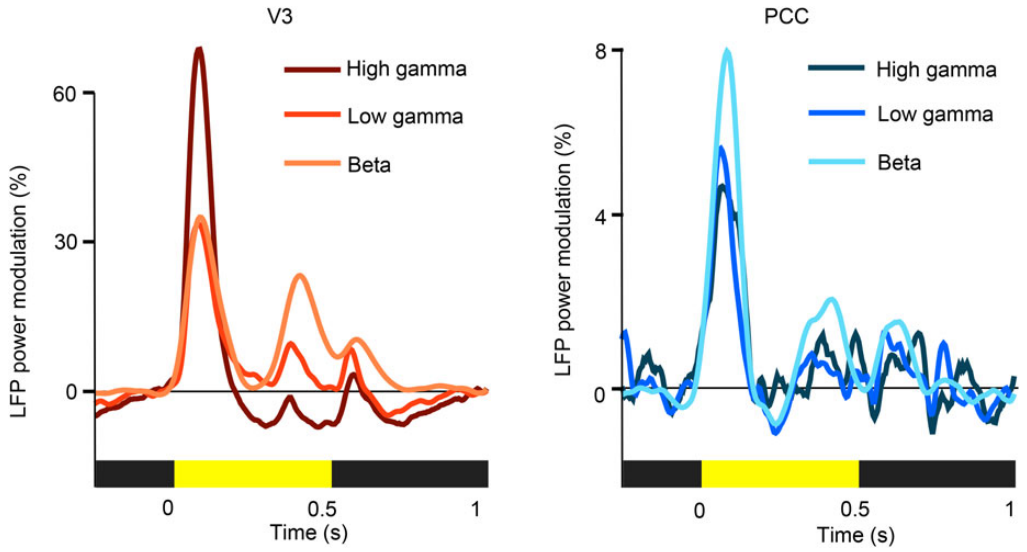

Figure 4. Flash-triggered average of LFP power for fourth to fifteen flashes. V3 shows prominent transients at the onset of each flash, with additional structure just before and after flash offset. Surprisingly, PCC also shows single-flash responses. The initial transients to the first flash (which are not included in this average; nor the second nor third flashes) are comparable in size with the V3 transients, but the later responses are ~10 times smaller.

PCC. In V3, the highest correlation coefficient was 0.68, occurring at a lag of 3.1 s. In PCC, the highest correlation was 0.72 at a lag of 4.3 s. These correlation values are slightly higher than those reported in previous studies, though the lags are similar (Mukamel 2005; Goense and Logothetis 2008; Murayama et al. 2010; Magri et al. 2012). The lag in PCC was significantly longer than that in V3 ($P < 0.0001$).

To further quantify the relationship between oxygen and LFP signals, we used 3 classes of functions to predict the oxygen response based on the gamma-band LFP response (50–100 Hz, spanning both low-gamma band and high-gamma band). We convolved the gamma-band LFP signal with each candidate function, adjusting parameters to minimize the mean-squared error between the result and the observed oxygen response. First, we used a canonical HRF used extensively in the BOLD-fMRI literature (see Materials and Methods) (Fig. 5, top 2 rows). Fits were performed by adjusting a single-scale parameter for each area (see Materials and Methods for details). The best-fit prediction explains a significant portion of variance in PCC ($r^2 = 0.85$) but only half of the variance in V3 ($r^2 = 0.53$). In each area, the predicted response (red and blue lines, far right column) fails to capture the initial onset response and subsequent transients (shading). Because of the poor fit with the 1-parameter function, we next tried a generic HRF with 8 free parameters (see Materials and Methods). The 8-parameter fit did well in both areas (Rows 3 and 4), though significantly better in PCC than V3 ($r^2 = 0.94$ in PCC, $r^2 = 0.85$ in V3, $P < 0.05$). Finally, we estimated a true transfer function using a variant of Fourier deconvolution (see Materials and Methods). As expected, the computed transfer function performed well in each area.

With each of the 3 classes of functions used to predict oxygen level, the best-fit function (Column 2) differed substantially between regions. For the canonical HRF (1-parameter fit, Rows 1 and 2), the scale parameter was 3.5 times larger in PCC than V3, a significant difference (as seen in the difference in the height of the orange versus cyan curves in Column 2; $P < 0.005$). With the generic HRF (8-parameter fit, Rows 3 and 4), the function shapes were very different in the two areas. The best fit for PCC had a prominent initial negativity compared with the V3 fit, and the scale parameter was again significantly greater for PCC compared with V3 (3.5 times, $P < 0.005$). Finally, the calculated transfer functions also were very different in the two areas (Rows 5 and 6). As with the 8-parameter fits, the transfer function for PCC showed an initial negativity that was not present in V3, and the overall amplitude was much larger for PCC than for V3. The difference in the transfer function between V3 and PCC was present in both monkeys, although there were differences in the exact shape of the transfer function in each individual animal (Supplementary Fig. 9).

These results demonstrate that the linear transfer function from gamma-band LFP power to oxygen level differs across areas. This result means that one or more of the following are true: hemodynamic coupling differs in PCC and V3, coupling is not driven by or is not well correlated with gamma-band LFP power, or coupling involves a more complex (non-linear) transformation. Several previous studies have shown that multiple frequency bands are correlated with BOLD, independent of gamma-band power (Scheeringa et al. 2011; Hermes et al. 2012; Magri et al. 2012; Harvey et al. 2013). This was also the case for our data. We found that LFP was correlated with oxygen at most frequencies, with no single band standing out as correlated particularly better than all the others (Fig. 6*a*). In V3, both high (>16 Hz) and low (<8 Hz) frequencies were positively correlated with oxygen, and middle frequencies (8–16 Hz) were negatively correlated with oxygen. The correlation pattern (negative correlation around alpha band range) is consistent with previous studies of primary visual and motor cortex (task-positive areas) (Scheeringa et al. 2011; Hermes et al. 2012; Magri et al. 2012; Harvey et al. 2013). The highest correlation between LFP and oxygen ($r = 0.68$) was found at an LFP frequency of 58 Hz. However, this was not a clear peak; the correlation was nearly as high (>0.60) from 1 to 2 Hz and from 38 to 86 Hz. In PCC, the highest correlation ($r = 0.74$) was at 4 Hz. As in V3, this was not a clear peak, with correlations of >0.60 from 1 to 12 Hz and from 58 to 150 Hz. Note that in PCC, all frequencies (including alpha band) were positively correlated with oxygen, which is a different correlation pattern compared with V3. The fact that alpha band LFP is negatively correlated with oxygen in V3 but positively

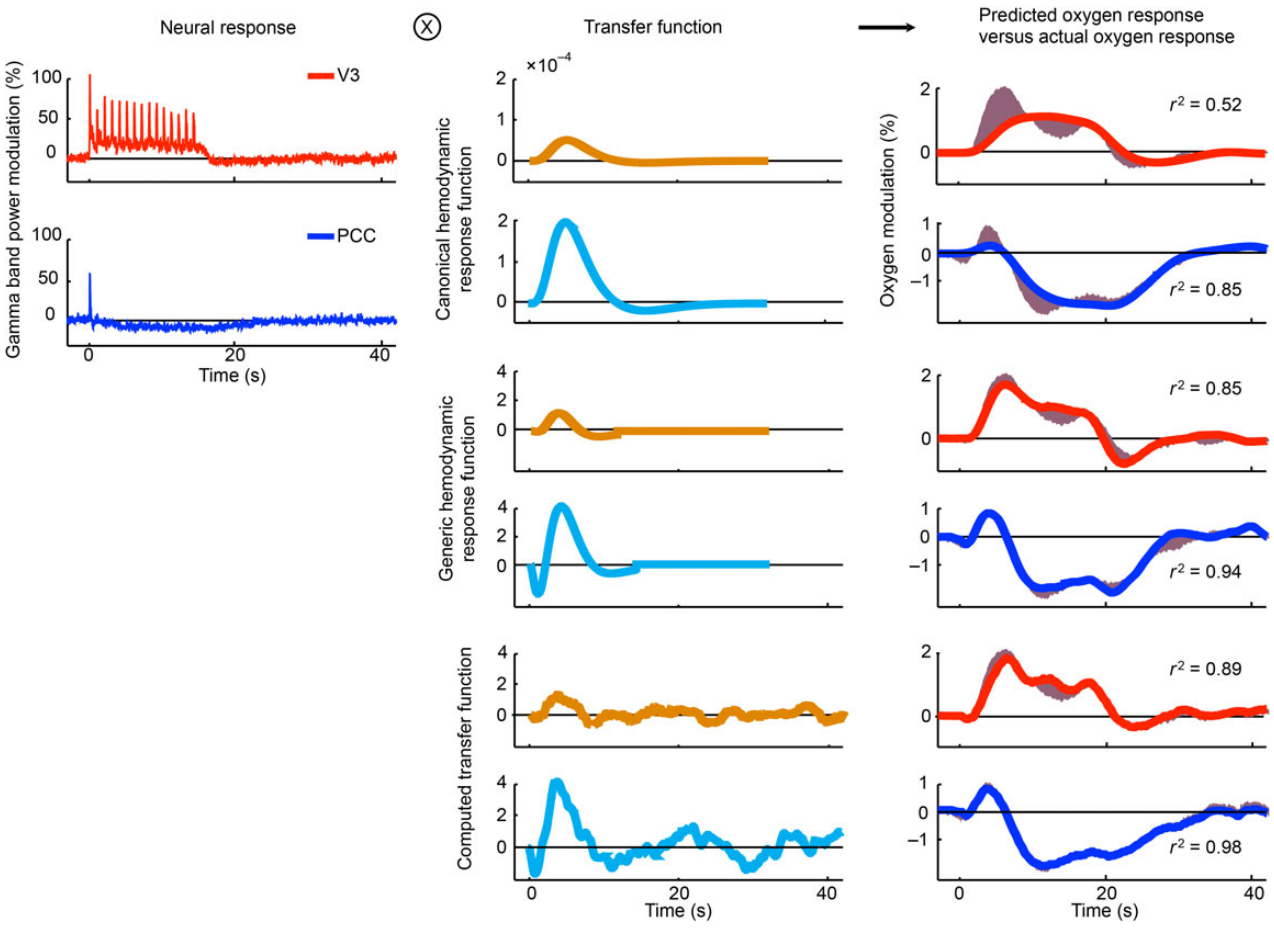

Figure 5. Hemodynamic coupling in V3 and PCC. First column: gamma-band LFP power in V3 (red) and PCC (blue). Second column: candidate transfer functions used to predict the oxygen response (third column) based on the LFP response (first column). The units of measure are percent oxygen modulation divided by percent LFP power modulation. Third column: predicted and actual oxygen responses. The predicted response is the convolution of the neural response (first column) with the selected transfer function (second column). Shading highlights any mismatch between the predicted and actual oxygen responses. Rows 1 + 2: A single parameter canonical HRF (canonical HRF; see text), fit to either the V3 (orange in the second column) or PCC data (cyan in the second column), is much smaller in V3 than PCC. Only 53% of the variance in the V3 oxygen signal can be predicted, and the initial transients are missed in both areas. Note that the scale parameter for the function is 3.5 times larger in PCC than V3 (as seen in the height of the orange versus cyan curves in Column 2). Rows 3 + 4: The best-fitting 8-parameter generic HRFs (see text) do well but have different shapes in the 2 areas. The fit for V3 (orange in the second column) has much smaller amplitude whereas the fit for PCC (cyan in the second column) contains an initial negativity that is not present in V3. Rows 5 + 6: A computed transfer function (see text) does well in both areas but, like the 8-parameter fits, is smaller in V3 (orange in the second column) and contains an initial negativity only in PCC (cyan in the second column).

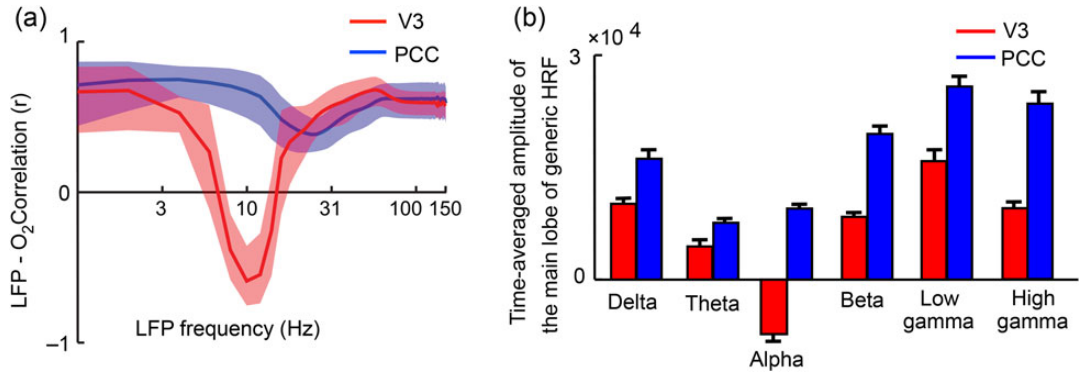

Figure 6. (*a*) A linear correlation (mean ± SEM) between oxygen and LFP responses at each frequency. Correlations were computed at lags from −5 to +12 s, and the highest correlation at each frequency is shown. (*b*) The amplitude (mean ± SEM) of the main lobe of generic HRFs in V3 and PCC at each of 6 frequency bands. Generic HRF was calculated for each data session, and the main lobe was defined as the lobe with the larger deviation from baseline. For all 6 bands, the amplitude of the main lobe of generic HRFs are significantly different in the 2 areas.

correlated with oxygen in PCC suggests that, if a linkage exists, it differs between the 2 areas.

Since the oxygen signal changed smoothly while the LFP power envelope changed rapidly and correlation may have been reduced by mismatched frequency content, we recomputed the correlations after 1-Hz low-pass filtering of the LFP power. This filtering had only a minimal effect on correlation. Even after low-pass filtering, no single LFP frequency or band in either area emerged as clearly better correlated with the oxygen signal than the other LFP frequencies.

Having confirmed that many LFP bands were correlated with oxygen level, not just gamma, we asked whether *any* LFP band showed a relationship with oxygen that was similar in V3 and PCC. We repeated the analysis of Figure 5 for each area and for each LFP band. In no case were the fit parameters or transfer function similar for the two areas (Fig. 6*b*).

Several previous studies have suggested that a combination of alpha band and gamma band may better explain oxygen responses, and the combination may lead to a consistent transfer function across areas (Scheeringa et al. 2011; Hermes et al. 2012; Magri et al. 2012; Harvey et al. 2013). We tested this idea by computing the transfer function using a combination of gamma power and the negative of alpha power. The negative sign for alpha power is to be consistent with the negative correlation between alpha power and BOLD (Scheeringa et al. 2011; Hermes et al. 2012; Magri et al. 2012; Harvey et al. 2013). The resulting transfer functions differed greatly between two areas, even more than the transfer functions based on gamma band power alone (data not shown).

In sum, quantification of the LFP–oxygen relationship demonstrated a strong link between neural and oxygen activity. Gamma band LFP power, as well as the power at most other frequencies, was linearly correlated with oxygen level in both V3 and PCC. However, the best-fit linear transfer function for PCC was substantially different from the best-fit function for V3 at every frequency from 1 to 150 Hz. These results suggest that either the nature of the relationship between neural activity and oxygen level differs between brain areas (Sloan et al. 2010; Conner et al. 2011) or that evaluating the relationship between the power modulation of single LFP frequency bands between 1 to 150 Hz and oxygen misses the mark and does not capture the true neural correlate of the oxygen response (see Discussion).

Discussion

We recorded local oxygen level and LFPs using oxygen polarography and electrophysiology in the awake macaque. Visually driven polarographic oxygen responses in both V3 and PCC were similar to BOLD fMRI responses obtained under similar conditions (Boynton et al. 1996; Logothetis et al. 2001; Lustig et al. 2003). This result indicates that oxygen polarography is a high resolution, electrophysiologically compatible surrogate for BOLD fMRI. Attention to a visual stimulus suppresses both oxygen level and LFP power in PCC compared with a "resting" baseline, demonstrating that macaques not only have a DMN, as previously described in resting state fMRI studies (Vincent et al. 2007), but also that the PCC exhibits a reduction in electrophysiological activity and oxygen level when the monkey engages with the external environment. Finally, oxygen and LFP responses were correlated in both V3 and PCC. However, the nature of the linear LFP–oxygen relationship differed substantially across regions (Ekstrom et al. 2009). These results demonstrate that either hemodynamic coupling differs in PCC and V3 or that a simple (linear, single LFP band) transformation is inappropriate for predicting oxygen level from neuronal activity.

Oxygen Polarography and BOLD fMRI

Oxygen polarography and BOLD fMRI both reflect oxygen level in the brain. BOLD fMRI signal intensity reflects the inverse magnitude of local magnetic field distortions caused by deoxyhemoglobin (Ogawa, Lee, Kay, et al. 1990; Ogawa, Lee, Nayak, et al. 1990; Menon et al. 1992). The concentration of deoxyhemoglobin is inversely related to blood oxygen (Kim and Bandettini 2011). Oxygen polarography measures available oxygen around the tip of the electrode, which in our study sits in tissue, not blood (Davies and Brink 1942; Thompson 2005). However, blood and tissue oxygen are generally in equilibrium and BOLD and polarographic oxygen signals should track one another (Mintun et al. 2001).

In practice, we find this to be true: polarographic oxygen closely resembles human BOLD fMRI responses obtained under similar conditions (Fig. 1). The oxygen time-course in V3 is similar to that observed in humans in response to sustained visual stimulation in early visual areas (Boynton et al. 1996; Volkow et al. 1997; Haynes et al. 2004; Fox et al. 2005; Uludağ 2008; Horiguchi et al. 2009; Mayhew et al. 2010) and is consistent with previous data from macaques (Logothetis et al. 1999, 2001; Vanduffel et al. 2001). Each of these studies shows a sustained BOLD response. A few also show an initial phasic response (Fox et al. 2005; Uludağ 2008; Horiguchi et al. 2009; Mayhew et al. 2010). The presence of a phasic response may depend on the specifics of the visual stimulus. For example, Uludağ (2008) shows both a phasic response and a sustained response in response to a long duration stimuli (20 s of stimulation followed by a 40 s of darkness), whose temporal structure is similar to the current study. The PCC oxygen time-course is also consistent with human data (Shulman, Corbetta, et al. 1997; Binder et al. 1999; Konishi et al. 2001; Mazoyer et al. 2001; Fox et al. 2005). Thus, to a first order, polarography and BOLD fMRI provide comparable measurements.

Polarographic and BOLD fMRI measurements operate at widely different spatial and temporal scales. Owing to physiologic (vascular) and technical limits, BOLD fMRI at 3 Tesla (3 T) is commonly limited to sampling volumes of 2–3 mm on a side at 1- to 3-s intervals, though spatial resolutions of up to 1 mm on a side and temporal resolutions of up to 2.5 Hz (with 2 mm voxels) are possible (De Martino et al. 2013; Xu et al. 2013). In contrast, our polarographic system samples spherical volumes of 30–100 μm in diameter, which are more than 3 orders of magnitude finer than BOLD voxels. Temporal frequency is limited by a low-pass-filter set to 20 Hz. The higher temporal resolution of polarography can resolve potential changes in oxygen level within the capillary bed that are invisible to fMRI (Kim and Bandettini 2011). It also improves our ability to separate neural signals from artifact generated by head motion and cardio-pulmonary pulsations (Birn 2012; Griffanti et al. 2014).

Oxygen polarography shares limitations with intracranial electrophysiology (e.g., limited coverage, invasiveness, and a requirement to stabilize the head) but also offers significant advantages. Awake macaque fMRI requires significant training to control animal behavior in the fMRI environment, requires that the animal keep still during data collection, and makes rewarding the animal problematic, since any movement that accompanies accepting a reward, even swallowing, will substantially degrade the fMRI signal. This severely limits animal experiments that can be performed with BOLD fMRI. In contrast, oxygen polarography is relatively insensitive to movement. Moreover, adding

electrophysiological recording to BOLD fMRI is technically demanding, whereas adding electrophysiology to polarography is straightforward and provides a match of the spatial specificity of the two signals that is difficult to achieve with fMRI.

The Default Mode Network in Monkeys

Only two of the many imaging studies in monkeys have reported a key feature of the human DMN: suppressed activity during external engagement compared with a resting state (Kojima et al. 2009; Mantini et al. 2011). In one of these studies, the data differed substantially across subjects, and the other required a meta-analysis of 8 independent studies in order to reveal the effects. This would seem to suggest that task-negative responses in monkey DMN are less robust than those in human DMN. However, our polarographic study provides evidence that this failure reflects a methodological issue rather than a true species difference. Adult humans can be verbally instructed to remain still in the magnet, but monkeys must be specifically trained and then periodically rewarded to remain still. A simple fixation task appears to be far more effortful for even a well-trained animal than for a human (unpublished observations based on error rates in trained subjects). We suggest that sitting still and maintaining fixation in the expectation of reward requires, in a monkey, substantially more engagement with the external environment than a similar task in a human. If this is true, then the failure of previous studies to demonstrate a robust negative BOLD response in PCC may reflect their use of an inadequate task-negative condition, that is, a task condition that required substantial engagement of the animal with the external environment.

In this study, we used tasks that were more suitable for producing a large contrast between states. With a long interstimulus interval and without the requirement to remain still and fixate for a reward, macaques naturally rest, reducing their engagement with the external environment. When this resting state was interrupted by an externally engaging visual stimulus, we observed clear suppressions in local oxygen level, LFP power, and multi-unit activity in PCC (Supplementary Fig. 10). These results demonstrate that simian and human DMNs are both markedly more active at rest than during external engagement. It is true that the "task" in our study was merely passive viewing of a visual stimulus. The animals were not required to perform any particular action. However, we observed, and confirmed via eye tracking, that animals oriented toward the stimulus on the majority of trials. Orienting toward a target is prima facie evidence that some degree of attention has been allocated. In any case, our results indicate that an engaging stimulus, compared with a period of no stimulation, is sufficient in the monkey to evoke a negative oxygen response in PCC. More generally, our results demonstrate the potential for our oxygen polarographic platform, deployed under various experimental conditions, to investigate the functions of the macaque DMN and in particular which functions, or what neural activity, correlate with BOLD activity.

Neural Basis of BOLD Responses

The physiological basis of task-induced positive BOLD responses is relatively well understood (Kim and Ogawa 2012; Lauritzen et al. 2012). Increased neural activity leads to an increase in metabolic demand, followed by an increase in oxygen supply via an increase in blood flow. The increase in oxygen supply exceeds the increase in oxygen consumption, leading to a decrease in the local concentration of deoxyhemoglobin and, hence, an increase in the T2*-weighted fMRI (BOLD) signal.

The physiological basis of task-induced negative BOLD responses, like those we report here, may be more complicated (Kim et al. 2014). However, the most straightforward view is that the mechanism accounted for task-negative responses is similar to the mechanism for task-induced positive responses. In support of this view, a handful of studies have reported task-related suppression of electrophysiological activity in default mode regions (Hayden et al. 2009; Jerbi 2010; Dastjerdi et al. 2011; Ossandon et al. 2011; Foster et al. 2012; Ramot et al. 2012; Gabbott and Rolls 2013). However, none report BOLD or oxygen responses under matched conditions, and the tasks used had very different temporal structure than those used in typical imaging studies of the default network (but see [Foster et al. 2012; Ramot et al. 2012]). We observed concomitant oxygen level and LFP power decreases during visual stimulation in PCC (Figs 1–3). LFPs are thought to reflect synchronized currents within spatially aligned dendrites from both excitatory and inhibitory neurons (Heeger and Ress 2002). Thus, our results support the hypothesis that default mode BOLD suppression reflects suppression of neural activity and a concomitant decrease in oxygen supply.

In PCC, we observed an initial increase in both oxygen level and LFP power in response to stimulus onset followed by sustained suppression (Fig. 1). The initial increase in oxygen was identical to that seen in V3, which is especially notable given the high temporal resolution of our method. Similar increases have been previously observed in human fMRI (Konishi et al. 2001; Lustig et al. 2003; Fox et al. 2005; Dosenbach et al. 2006; Yarkoni et al. 2008; Sambataro et al. 2010). We also observed phasic increases in LFP power within PCC with each flash of the visual stimulus (Fig. 4). The initial and subsequent phasic increases in LFP power suggest that at least two neural processes, one task-positive and one task-negative, co-exist in PCC during visual stimulation.

Neuro-Hemodynamic Coupling

Our analysis suggests that the relationship between oxygen and LFP differs across areas (Figs 5 and 6*b*). For example, the linear transfer function relating gamma-band power with oxygen contains an early negativity for PCC but not V3 (Fig. 5, Row 6, middle column). The early decrease in oxygen in response to a stimulus may reflect a local increase in oxygen consumption that precedes an increase in regional blood flow (Malonek and Grinvald 1996; Kim et al. 2000; Thompson et al. 2003). Alternatively, the initial negativity in the PCC transfer function could reflect a linear approximation to a complex non-linear relationship. The BOLD response to repeated stimuli presented closely together in time is non-linear (Friston et al. 1998) (although Siero et al. attribute most of this non-linearity to neuronal processes [Siero et al. 2013]). Different non-linearities in PCC versus V3 could give rise to an initial negativity in one function but not the other.

More generally, we assumed in our analysis that neurovascular coupling was a linear process involving a single LFP frequency band. A more complete analysis would consider non-linear combinations of all LFP bands, including those well below 1 Hz, multi- and single-unit activity and phase relationship between units and field potentials. Such an analysis is confounded by the infinite number of possible non-linear transformations, which guarantee the ability to find transfer functions that are identical across areas (See Supplementary Text for an illustration). To avoid this confound, transformations would need to be cross-validated using data collected under different experimental conditions.

Following changes in neural activity, cerebral blood flow, cerebral blood volume, and cerebral metabolic rate of oxygen ($CMRO_2$)

all change with different spatial and temporal dynamics. Each of these factors may influence tissue oxygen level. In this study, we show a scale difference in the relationship between oxygen and LFP in V3 compared with PCC; however, further work is required to determine which factor(s) contribute to the scale difference.

In conclusion, we demonstrate that oxygen and LFP responses are closely related to each other in both V3 and PCC (Figs 1 and 2*a*), supporting the idea that oxygen level and neural activity are closely related to each other in both V3 and PCC. A simple linear transformation of gamma-band LFP power accounts for 85% of the variance in the oxygen signal in our task (Fig. 5, Rows 3 and 4). The relationship is not specific to the gamma band but instead is present over a wide range of LFP frequencies (Fig. 6*a*). Finally, we show that the details of the relationship between oxygen and LFP responses differ across areas, at least for single-frequency band, linear transformations (Fig. 5). For example, an initial negativity is present in the PCC transfer function but not in the V3 transfer function, and the computed hemodynamic efficiency (the ratio of how much oxygen level changes for a given change in LFP power) is 2–4 times greater in PCC than that in V3 (Figs 5 and 6*b*). This implies that the relationship between neural activity and oxygen either varies across regions, is a non-linear function of LFP power, reflects frequencies outside of the standard LFP range, or some combination of these possibilities. The ability to combine polarographic oxygen recording with electrophysiological recording in the awake behaving primate provides a platform for testing each possibility.

Author Contributions

W.J.B., J.M.L., A.Z.S., M.R., and L.H.S. designed the research; W.J.B. and J.M.L. performed the research; W.J.B. and J.M.L. analyzed the data; and W.J.B., J.M.L., A.Z.S., M.R. and L.H.S. wrote the paper.

Supplementary Material

Supplementary material can be found at: http://www.cercor.oxfordjournals.org/.

Funding

This research was supported by NIH R21 MH093858 and NIH R01 MH102471.

Notes

We thank Drs. Timothy Holy and ShiNung Ching for helpful discussions on data analysis; Drs. Todd Braver and Grega Repovs for comments on an earlier version of the manuscript. *Conflict of Interest*: None declared.

References

Anticevic A, Cole MW, Murray JD, Corlett PR, Wang XJ, Krystal JH. 2012. The role of default network deactivation in cognition and disease. Trends Cogn Sci. 16:584–592.

Bartolo MJ, Gieselmann MA, Vuksanovic V, Hunter D, Sun L, Chen X, Delicato LS, Thiele A. 2011. Stimulus-induced dissociation of neuronal firing rates and local field potential gamma power and its relationship to the resonance blood oxygen level-dependent signal in macaque primary visual cortex. Eur J Neurosci. 34:1857–1870.

Binder JR, Frost JA, Hammeke TA, Bellgowan PS, Rao SM, Cox RW. 1999. Conceptual processing during the conscious resting state. A functional MRI study. J Cogn Neurosci. 11:80–95.

Birn RM. 2012. The role of physiological noise in resting-state functional connectivity. NeuroImage. 62:864–870.

Boynton GM, Engel SA, Glover GH, Heeger DJ. 1996. Linear systems analysis of functional magnetic resonance imaging in human V1. J Neurosci. 16:4207–4221.

Bronk DW, Larrabee MG, Davies PW. 1946. The rate of oxygen consumption in localized regions of the nervous system: in presynaptic endings and in cell bodies. Fed Proc. 5:11.

Buckner RL, Andrews-Hanna JR, Schacter DL. 2008. The brain's default network: anatomy, function, and relevance to disease. Ann N Y Acad Sci. 1124:1–38.

Clark LC Jr, Wolf R, Granger D, Taylor Z. 1953. Continuous recording of blood oxygen tensions by polarography. J Appl Physiol. 6:189–193.

Conner CR, Ellmore TM, Pieters TA, DiSano MA, Tandon N. 2011. Variability of the relationship between electrophysiology and BOLD-fMRI across cortical regions in humans. J Neurosci. 31:12855–12865.

Dastjerdi M, Foster BL, Nasrullah S, Rauschecker AM, Dougherty RF, Townsend JD, Chang CT, Greicius MD, Menon V, Kennedy DP, et al. 2011. Differential electrophysiological response during rest, self-referential, and non-self-referential tasks in human posteromedial cortex. Proc Natl Acad Sci USA. 108:3023–3028.

Davies PW, Brink F. 1942. Microelectrodes for measuring local oxygen tension in animal tissues. Rev Sci Instrum. 13:524–533.

De Martino F, Zimmermann J, Muckli L, Ugurbil K, Yacoub E, Goebel R. 2013. Cortical depth dependent functional responses in humans at 7T: improved specificity with 3D GRASE. PloS One. 8:e60514.

Devor A, Tian PF, Nishimura N, Teng IC, Hillman EMC, Narayanan SN, Ulbert I, Boas DA, Kleinfeld D, Dale AM. 2007. Suppressed neuronal activity and concurrent arteriolar vasoconstriction may explain negative blood oxygenation level-dependent signal. J Neurosci. 27:4452–4459.

Dosenbach NUF, Visscher KM, Palmer ED, Miezin FM, Wenger KK, Kang HC, Burgund ED, Grimes AL, Schlaggar BL, Petersen SE. 2006. A core system for the implementation of task sets. Neuron. 50:799–812.

Ekstrom A, Suthana N, Millett D, Fried I, Bookheimer S. 2009. Correlation between BOLD fMRI and theta-band local field potentials in the human hippocampal area. J Neurophysiol. 101:2668–2678.

Fatt I. 1976. Polarographic Oxygen Sensors. Cleveland, Ohio: CRC Press.

Foster BL, Dastjerdi M, Parvizi J. 2012. Neural populations in human posteromedial cortex display opposing responses during memory and numerical processing. Proc Natl Acad Sci USA. 109:15514–15519.

Foster BL, Parvizi J. 2012. Resting oscillations and cross-frequency coupling in the human posteromedial cortex. NeuroImage. 60:384–391.

Fox MD, Snyder AZ, Barch DM, Gusnard DA, Raichle ME. 2005. Transient BOLD responses at block transitions. NeuroImage. 28:956–966.

Fox MD, Snyder AZ, Vincent JL, Corbetta M, Van Essen DC, Raichle ME. 2005. The human brain is intrinsically organized into dynamic, anticorrelated functional networks. Proc Natl Acad Sci USA. 102:9673–9678.

Friston KJ, Josephs O, Rees G, Turner R. 1998. Nonlinear event-related responses in fMRI. Magn Reson Med. 39:41–52.

Gabbott PL, Rolls ET. 2013. Increased neuronal firing in resting and sleep in areas of the macaque medial prefrontal cortex. Eur J Neurosci. 37:1737–1746.

Goense JB, Logothetis NK. 2008. Neurophysiology of the BOLD fMRI signal in awake monkeys. Curr Biol. 18:631–640.

Greicius MD, Krasnow B, Reiss AL, Menon V. 2003. Functional connectivity in the resting brain: a network analysis of the default mode hypothesis. Proc Natl Acad Sci USA. 100:253–258.

Griffanti L, Salimi-Khorshidi G, Beckmann CF, Auerbach EJ, Douaud G, Sexton CE, Zsoldos E, Ebmeier KP, Filippini N, Mackay CE, et al. 2014. ICA-based artefact removal and accelerated fMRI acquisition for improved resting state network imaging. NeuroImage. 95C:232–247.

Harvey BM, Vansteensel MJ, Ferrier CH, Petridou N, Zuiderbaan W, Aarnoutse EJ, Bleichner MG, Dijkerman HC, van Zandvoort MJ, Leijten FS, et al. 2013. Frequency specific spatial interactions in human electrocorticography: V1 alpha oscillations reflect surround suppression. NeuroImage. 65: 424–432.

Hayden BY, Smith DV, Platt ML. 2009. Electrophysiological correlates of default-mode processing in macaque posterior cingulate cortex. Proc Natl Acad Sci USA. 106:5948–5953.

Haynes J-D, Lotto RB, Rees G. 2004. Responses of human visual cortex to uniform surfaces. Proc Natl Acad Sci. 101: 4286–4291.

He BYJ, Snyder AZ, Zempel JM, Smyth MD, Raichle ME. 2008. Electrophysiological correlates of the brain's intrinsic large-scale functional architecture. Proc Natl Acad Sci USA. 105: 16039–16044.

Heeger DJ, Ress D. 2002. What does fMRI tell us about neuronal activity? Nat Rev Neurosci. 3:142–151.

Hermes D, Miller KJ, Vansteensel MJ, Aarnoutse EJ, Leijten FS, Ramsey NF. 2012. Neurophysiologic correlates of fMRI in human motor cortex. Hum Brain Mapp. 33:1689–1699.

Horiguchi H, Nakadomari S, Misaki M, Wandell BA. 2009. Two temporal channels in human V1 identified using fMRI. NeuroImage. 47:273–280.

Jerbi 2010. Exploring the electrophysiological correlates of the default-mode network with intracerebral EEG. Front Syst Neurosc. 4:27.

Kayser C. 2004. A comparison of hemodynamic and neural responses in cat visual cortex using complex stimuli. Cereb Cortex. 14:881–891.

Kim DS, Duong TQ, Kim SG. 2000. High-resolution mapping of iso-orientation columns by fMRI. Nat Neurosci. 3:164–169.

Kim R, Hyder F, Blumenfeld H. 2014. Physiological basis of BOLD fMRI decreases. In: Zhao M, Ma H, Schwartz TH, editors. Neurovascular Coupling Methods. New York: Springer. p. 221–236.

Kim S-G, Bandettini PA. 2011. Principles of BOLD functional MRI. In: Boston, MA: Springer US. p. 293–303.

Kim SG, Ogawa S. 2012. Biophysical and physiological origins of blood oxygenation level-dependent fMRI signals. J Cereb Blood Flow Metab. 32:1188–1206.

Kojima T, Onoe H, Hikosaka K, Tsutsui K, Tsukada H, Watanabe M. 2009. Default mode of brain activity demonstrated by positron emission tomography imaging in awake monkeys: higher rest-related than working memory-related activity in medial cortical areas. J Neurosci. 29:14463–14471.

Konishi S, Donaldson DI, Buckner RL. 2001. Transient activation during block transition. NeuroImage. 13:364–374.

Kwong KK, Belliveau JW, Chesler DA, Goldberg IE, Weisskoff RM, Poncelet BP, Kennedy DN, Hoppel BE, Cohen MS, Turner R, et al. 1992. Dynamic magnetic resonance imaging of human brain activity during primary sensory stimulation. Proc Natl Acad Sci USA. 89:5675–5679.

Lauritzen M, Mathiesen C, Schaefer K, Thomsen KJ. 2012. Neuronal inhibition and excitation, and the dichotomic control of brain hemodynamic and oxygen responses. Neuroimage. 62:1040–1050.

Logothetis NK, Guggenberger H, Peled S, Pauls J. 1999. Functional imaging of the monkey brain. Nat Neurosci. 2:555–562.

Logothetis NK, Pauls J, Augath M, Trinath T, Oeltermann A. 2001. Neurophysiological investigation of the basis of the fMRI signal. Nature. 412:150–157.

Lowry JP, Griffin K, McHugh SB, Lowe AS, Tricklebank M, Sibson NR. 2010. Real-time electrochemical monitoring of brain tissue oxygen: a surrogate for functional magnetic resonance imaging in rodents. NeuroImage. 52:549–555.

Lu H, Zuo Y, Gu H, Waltz Ja, Zhan W, Scholl Ca, Rea W, Yang Y, Stein Ea. 2007. Synchronized delta oscillations correlate with the resting-state functional MRI signal. Proc Natl Acad Sci USA. 104:18265–18269.

Lustig C, Snyder AZ, Bhakta M, O'Brien KC, McAvoy M, Raichle ME, Morris JC, Buckner RL. 2003. Functional deactivations: change with age and dementia of the Alzheimer type. Proc Natl Acad Sci USA. 100:14504–14509.

Magri C, Schridde U, Murayama Y, Panzeri S, Logothetis NK. 2012. The amplitude and timing of the BOLD signal reflects the relationship between local field potential power at different frequencies. J Neurosci. 32:1395–1407.

Maier A, Wilke M, Aura C, Zhu C, Ye FQ, Leopold Da. 2008. Divergence of fMRI and neural signals in V1 during perceptual suppression in the awake monkey. Nat Neurosci. 11:1193–1200.

Malonek D, Grinvald A. 1996. Interactions between electrical activity and cortical microcirculation revealed by imaging spectroscopy: implications for functional brain mapping. Science. 272:551–554.

Mantini D, Corbetta M, Romani GL, Orban GA, Vanduffel W. 2013. Evolutionarily novel functional networks in the human brain? J Neurosci. 33:3259–3275.

Mantini D, Gerits A, Nelissen K, Durand JB, Joly O, Simone L, Sawamura H, Wardak C, Orban GA, Buckner RL, et al. 2011. Default mode of brain function in monkeys. J Neurosci. 31:12954–12962.

Masamoto K, Vazquez A, Wang P, Kim S-G. 2008. Trial-by-trial relationship between neural activity, oxygen consumption, and blood flow responses. NeuroImage. 40:442–450.

Mayhew SD, Macintosh BJ, Dirckx SG, Iannetti GD, Wise RG. 2010. Coupling of simultaneously acquired electrophysiological and haemodynamic responses during visual stimulation. Magn Reson Imag. 28:1066–1077.

Mazoyer B, Zago L, Mellet E, Bricogne S, Etard O, Houdé O, Crivello F, Joliot M, Petit L, Tzourio-Mazoyer N. 2001. Cortical networks for working memory and executive functions sustain the conscious resting state in man. Brain Res Bull. 54:287–298.

Menon RS, Ogawa S, Kim SG, Ellermann JM, Merkle H, Tank DW, Ugurbil K. 1992. Functional brain mapping using magnetic resonance imaging. Signal changes accompanying visual stimulation. Invest Radiol. 27 Suppl 2:S47–S53.

Mintun MA, Lundstrom BN, Snyder AZ, Vlassenko AG, Shulman GL, Raichle ME. 2001. Blood flow and oxygen delivery to human brain during functional activity: theoretical modeling and experimental data. Proc Natl Acad Sci. 98:6859–6864.

Mukamel R. 2005. Coupling between neuronal firing, field potentials, and fMRI in human auditory cortex. Science. 309: 951–954.

Murayama Y, Biessmann F, Meinecke FC, Muller KR, Augath M, Oeltermann A, Logothetis NK. 2010. Relationship between neural and hemodynamic signals during spontaneous activity studied with temporal kernel CCA. Magn Reson Imag. 28:1095–1103.

Niessing J. 2005. Hemodynamic signals correlate tightly with synchronized gamma oscillations. Science. 309:948–951.

Ogawa S, Lee TM, Kay aR, Tank DW. 1990. Brain magnetic resonance imaging with contrast dependent on blood oxygenation. Proc Natl Acad Sci USA. 87:9868–9872.

Ogawa S, Lee TM, Nayak AS, Glynn P. 1990. Oxygenation-sensitive contrast in magnetic resonance image of rodent brain at high magnetic fields. Magn Reson Med. 14:68–78.

Ogawa S, Tank DW, Menon R, Ellermann JM, Kim SG, Merkle H, Ugurbil K. 1992. Intrinsic signal changes accompanying sensory stimulation: functional brain mapping with magnetic resonance imaging. Proc Natl Acad Sci USA. 89: 5951–5955.

Ossandon T, Jerbi K, Vidal JR, Bayle DJ, Henaff MA, Jung J, Minotti L, Bertrand O, Kahane P, Lachaux JP. 2011. Transient suppression of broadband gamma power in the default-mode network is correlated with task complexity and subject performance. J Neurosci. 31:14521–14530.

Pan W-J, Thompson GJ, Magnuson ME, Jaeger D, Keilholz S. 2013. Infraslow LFP correlates to resting-state fMRI BOLD signals. NeuroImage. 74:288–297.

Press WHT, Saul A, Vetterling William T, Flannery Brain P. 2007. Numerical Recipes: The Art of Scientific Computing Third Edition. New York: Cambridge University Press.

Raichle ME, MacLeod aM, Snyder aZ, Powers WJ, Gusnard Da, Shulman GL. 2001. A default mode of brain function. Proc Natl Acad Sci USA. 98:676–682.

Ramot M, Fisch L, Harel M, Kipervasser S, Andelman F, Neufeld MY, Kramer U, Fried I, Malach R. 2012. A widely distributed spectral signature of task-negative electrocorticography responses revealed during a visuomotor task in the human cortex. J Neurosci. 32:10458–10469.

Rosa MJ, Kilner J, Blankenburg F, Josephs O, Penny W. 2010. Estimating the transfer function from neuronal activity to BOLD using simultaneous EEG-fMRI. NeuroImage. 49:1496–1509.

Saleem KS, Logothetis NK. 2007. A Combined MRI and Histology Atlas of the Rhesus Monkey Brain in Stereotaxic Coordinates. San Diego: Elsevier/Academic press.

Sambataro F, Murty VP, Callicott JH, Tan H-Y, Das S, Weinberger DR, Mattay VS. 2010. Age-related alterations in default mode network: impact on working memory performance. Neurobiol Aging. 31:839–852.

Scheeringa R, Fries P, Petersson KM, Oostenveld R, Grothe I, Norris DG, Hagoort P, Bastiaansen MC. 2011. Neuronal dynamics underlying high- and low-frequency EEG oscillations contribute independently to the human BOLD signal. Neuron. 69:572–583.

Shmuel A, Augath M, Oeltermann A, Logothetis NK. 2006. Negative functional MRI response correlates with decreases in neuronal activity in monkey visual area V1. Nat Neurosci. 9:569–577.

Shulman GL, Corbetta M, Buckner RL, Fiez JA, Miezin FM, Raichle ME, Petersen SE. 1997. Common blood flow changes across visual tasks: I. Increases in subcortical structures and cerebellum but not in nonvisual cortex. J Cogn Neurosci. 9:624–647.

Shulman GL, Fiez JA, Corbetta M, Buckner RL, Miezin FM, Raichle ME, Petersen SE. 1997. Common blood flow changes across visual tasks: II. Decreases in cerebral cortex. J Cogn Neurosci. 9:648–663.

Siero JC, Hermes D, Hoogduin H, Luijten PR, Petridou N, Ramsey NF. 2013. BOLD consistently matches electrophysiology in human sensorimotor cortex at increasing movement rates: a combined 7T fMRI and ECoG study on neurovascular coupling. J Cereb Blood Flow Metab. 33:1448–1456.

Singh KD. 2012. Which "neural activity" do you mean? fMRI, MEG, oscillations and neurotransmitters. NeuroImage. 62:1121–1130.

Sloan HL, Austin VC, Blamire AM, Schnupp JW, Lowe AS, Allers KA, Matthews PM, Sibson NR. 2010. Regional differences in neurovascular coupling in rat brain as determined by fMRI and electrophysiology. NeuroImage. 53:399–411.

Thompson JK. 2005. Separate spatial scales determine neural activity-dependent changes in tissue oxygen within central visual pathways. J Neurosci. 25:9046–9058.

Thompson JK, Peterson MR, Freeman RD. 2004. High-resolution neurometabolic coupling revealed by focal activation of visual neurons. Nat Neurosci. 7:919–920.

Thompson JK, Peterson MR, Freeman RD. 2003. Single-neuron activity and tissue oxygenation in the cerebral cortex. Science. 299:1070–1072.

Thomsen K, Piilgaard H, Gjedde A, Bonvento G, Lauritzen M. 2009. Principal cell spiking, postsynaptic excitation, and oxygen consumption in the rat cerebellar cortex. J Neurophysiol. 102:1503–1512.

Uludağ K. 2008. Transient and sustained BOLD responses to sustained visual stimulation. Magn Reson Imag. 26:863–869.

van den Heuvel MP, Sporns O. 2013. An anatomical substrate for integration among functional networks in human cortex. J Neurosci. 33:14489–14500.

Vanduffel W, Fize D, Mandeville JB, Nelissen K, Van Hecke P, Rosen BR, Tootell RBH, Orban GA. 2001. Visual motion processing investigated using contrast agent-enhanced fMRI in awake behaving monkeys. Neuron. 32:565–577.

Vincent JL, Patel GH, Fox MD, Snyder AZ, Baker JT, Van Essen DC, Zempel JM, Snyder LH, Corbetta M, Raichle ME. 2007. Intrinsic functional architecture in the anaesthetized monkey brain. Nature. 447:83–86.

Volkow ND, Rosen B, Farde L. 1997. Imaging the living human brain: magnetic resonance imaging and positron emission tomography. Proc Natl Acad Sci USA. 94:2787–2788.

Worsley KJ, Friston KJ. 1995. Analysis of fMRI time-series revisited – again. NeuroImage. 2:173–181.

Wu L, Eichele T, Calhoun VD. 2010. Reactivity of hemodynamic responses and functional connectivity to different states of alpha synchrony: a concurrent EEG-fMRI study. NeuroImage. 52:1252–1260.

Xu J, Moeller S, Auerbach EJ, Strupp J, Smith SM, Feinberg DA, Yacoub E, Ugurbil K. 2013. Evaluation of slice accelerations using multiband echo planar imaging at 3T. NeuroImage. 83:991–1001.

Yarkoni T, Speer NK, Zacks JM. 2008. Neural substrates of narrative comprehension and memory. NeuroImage. 41:1408–1425.

Supplementary Text

Given a single input and a single output, a linear transform relating the two can always be found (Press WHT, Saul A. Vetterling, William T. and Flannery, Brain P. 2007). With two sets of two inputs and two outputs, one can also always find a linear solution (proof to follow). For example, we might have both Gamma LFP power (input 1) and Alpha LFP power (input 2) from area V3 and from area PCC, and wish to find a set of linear transfer functions (TF1 and TF2) that relate these two inputs to the BOLD signals in each area (Output.a and Output.b). We can express this mathematically as follows:

$$\mathrm{Input1.a} * \mathrm{TF1} + \mathrm{Input2.a} * \mathrm{TF2} = \mathrm{Output.a} \quad (1)$$
$$\mathrm{Input1.b} * \mathrm{TF1} + \mathrm{Input2.b} * \mathrm{TF2} = \mathrm{Output.b} \quad (2)$$

Here each term is the time frequency representation of either LFP power (inputs) or the BOLD response (outputs). Multiplication in the frequency domain ("*") is the same as convolution in the time domain (Press WHT, Saul A. Vetterling, William T. and Flannery, Brain P. 2007). Solving for the two transfer functions yields:

$$\mathrm{TF1} = \frac{\mathrm{Output.a} * \mathrm{Input1.b} - \mathrm{Output.b} * \mathrm{Input1.a}}{\mathrm{Input2.a} * \mathrm{Input1.b} - \mathrm{Input2.b} * \mathrm{Input1.a}} \quad (3)$$
$$\mathrm{TF2} = \frac{\mathrm{Output.b} * \mathrm{Input2.a} - \mathrm{Output.a} * \mathrm{Input2.b}}{\mathrm{Input2.a} * \mathrm{Input1.b} - \mathrm{Input2.b} * \mathrm{Input1.a}} \quad (4)$$

A finite solution exists so long as

$$\mathrm{Input2.a} * \mathrm{Input1.b} \neq \mathrm{Input2.b} * \mathrm{Input1.a}$$

$$\rightarrow \quad \frac{\mathrm{Input1.a}}{\mathrm{Input1.b}} \neq \frac{\mathrm{Input2.a}}{\mathrm{Input2.b}} \quad (5)$$

In other words, if the ratio between Alpha and Gamma bands is not the same in V3 as it is in PCC, we are guaranteed to find a set of transfer functions that works for both V3 and PCC. More generally, we can replace Alpha and Gamma with any other pair of bands (for instance, Delta and Theta bands). Thus, by using two LFP bands, a mathematical solution can be found that will relate the LFP signals to the BOLD recorded in two different areas. However, given that this is guaranteed to work with any pair of LFP signals, it is doubtful that the solution will reflect anything of physiological interest.

Press WHT, Saul A. Vetterling, William T. and Flannery, Brain P. 2007. Numerical Recipes: The Art of Scientific Computing Third Edition. Cambridge University Press.

Supplementary Figure S1

Figure S1. Examples of visual stimuli used in this study. The projector we used to deliver the stimuli blurred the visual stimuli, to an extent equivalent to applying a 2-pixel radius Gaussian filter to a 259 X194 pixel image. Two examples are shown to illustrate the effect of the blurring.

Supplementary Figure S2

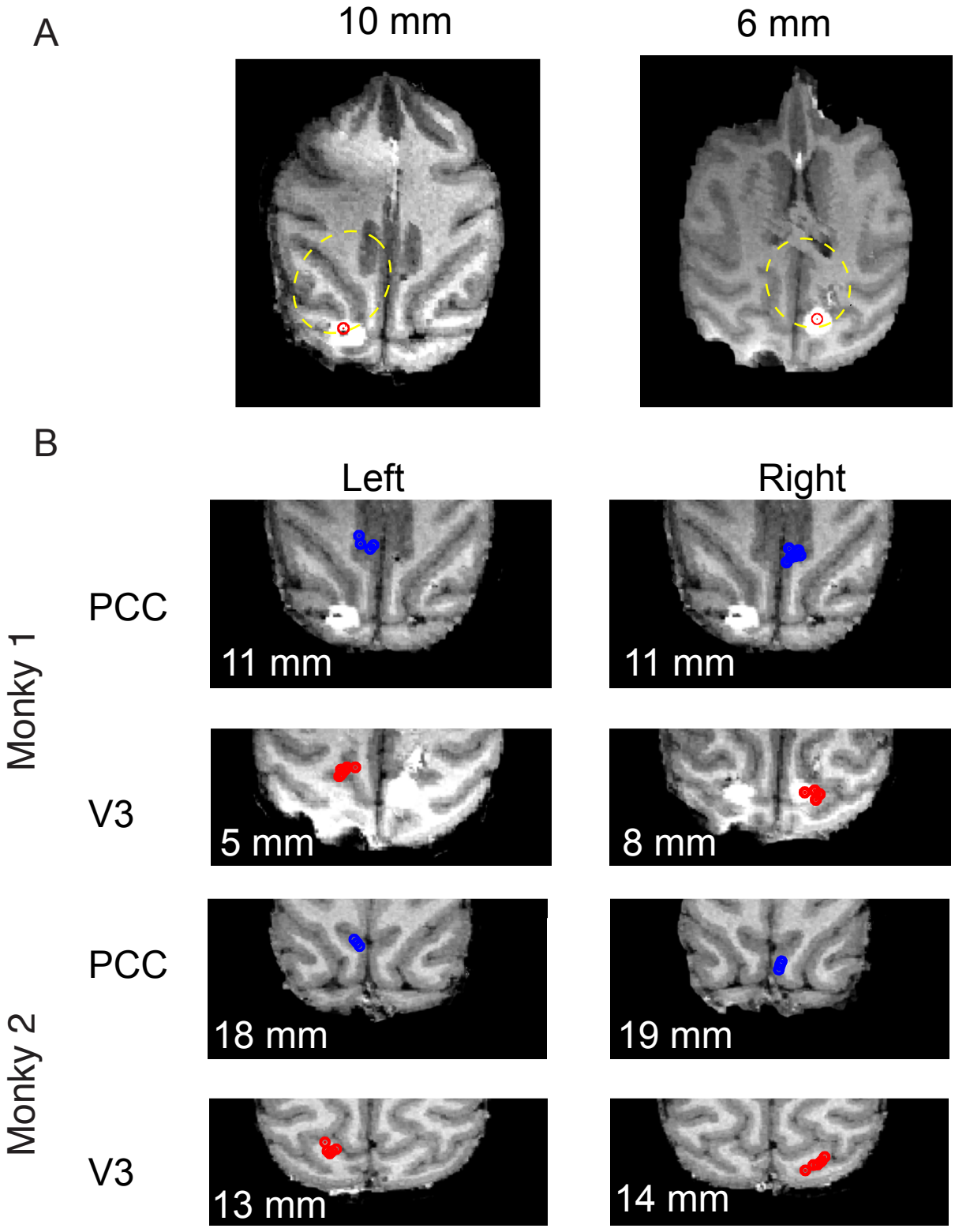

Figure S2. Recording sites confirmed by manganese injections. Manganese is MRI lucent and was used to calibrate our recording apparatus. A. MRI images showing injections into each hemisphere (white blobs) and the locations at which injections were aimed (red dots). The dots are aligned with the injections, confirming the accuracy of our maps. The dashed yellow ovals mark the boundaries of our recording chambers. B. Recording sites in the two monkeys (blue dots for PCC, and red dots for V3). Recordings into each hemisphere in each monkey are shown separately, often at a different slice depth. For example, the upper left panel shows PCC recordings into Monkey 1, left hemisphere. The slice depths indicate millimeters above the anterior commissure. The top of the brain is at 22 mm and 26 mm for Monkey 1 and Monkey 2, respectively.

Supplementary Figure S3

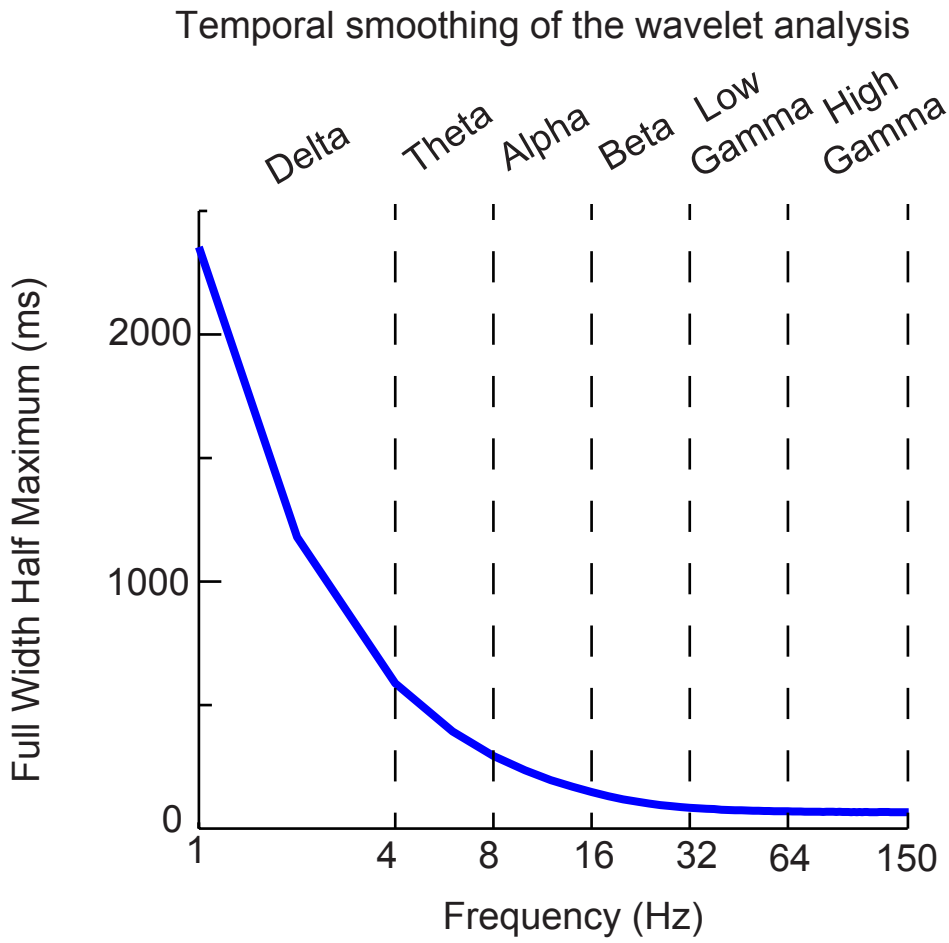

Figure S3. The temporal smoothing of the wavelet analysis. Power at specific frequency is estimated by convolving data with a complex Morlet wavelet. This method includes inherent low-pass temporal smoothing. The degree of smoothing is a function of frequency, and is similar to convolving the instantaneous power with a Gaussian. Here we show the full width of the equivalent Gaussian at half maximum height for each frequency. Notice that the degree of smoothing is greater for lower frequencies.

Supplementary Figure S4

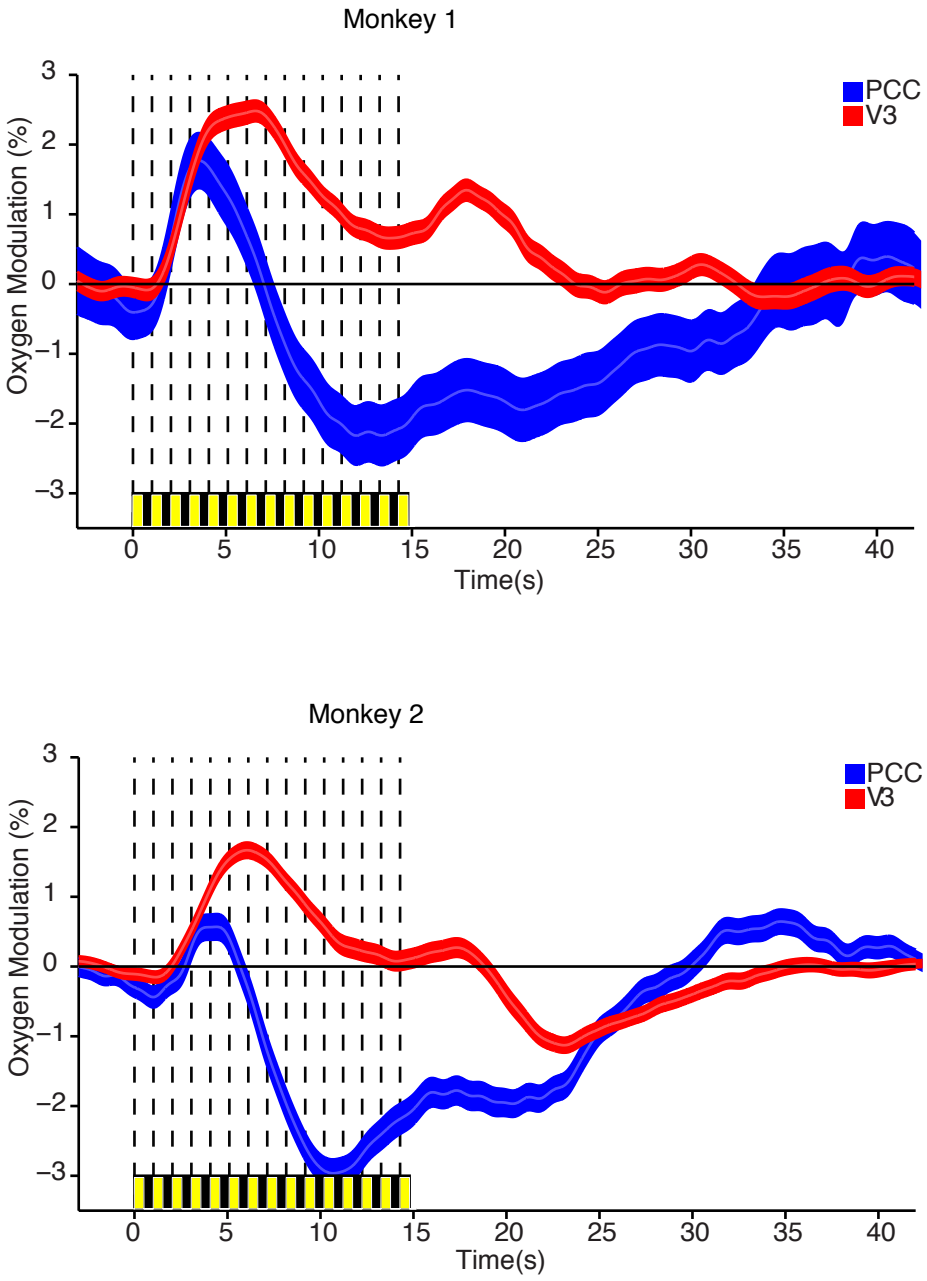

Figure S4. Percent oxygen modulation (mean ± SEM) relative to the period 0-5 s before stimulus onset for both monkeys. In V3, oxygen level shows a transient response to the stimulus onset, followed by sustained activation. In PCC, oxygen level shows transient activation followed by sustained suppression. These are true for both monkeys.

Supplementary Figure S5

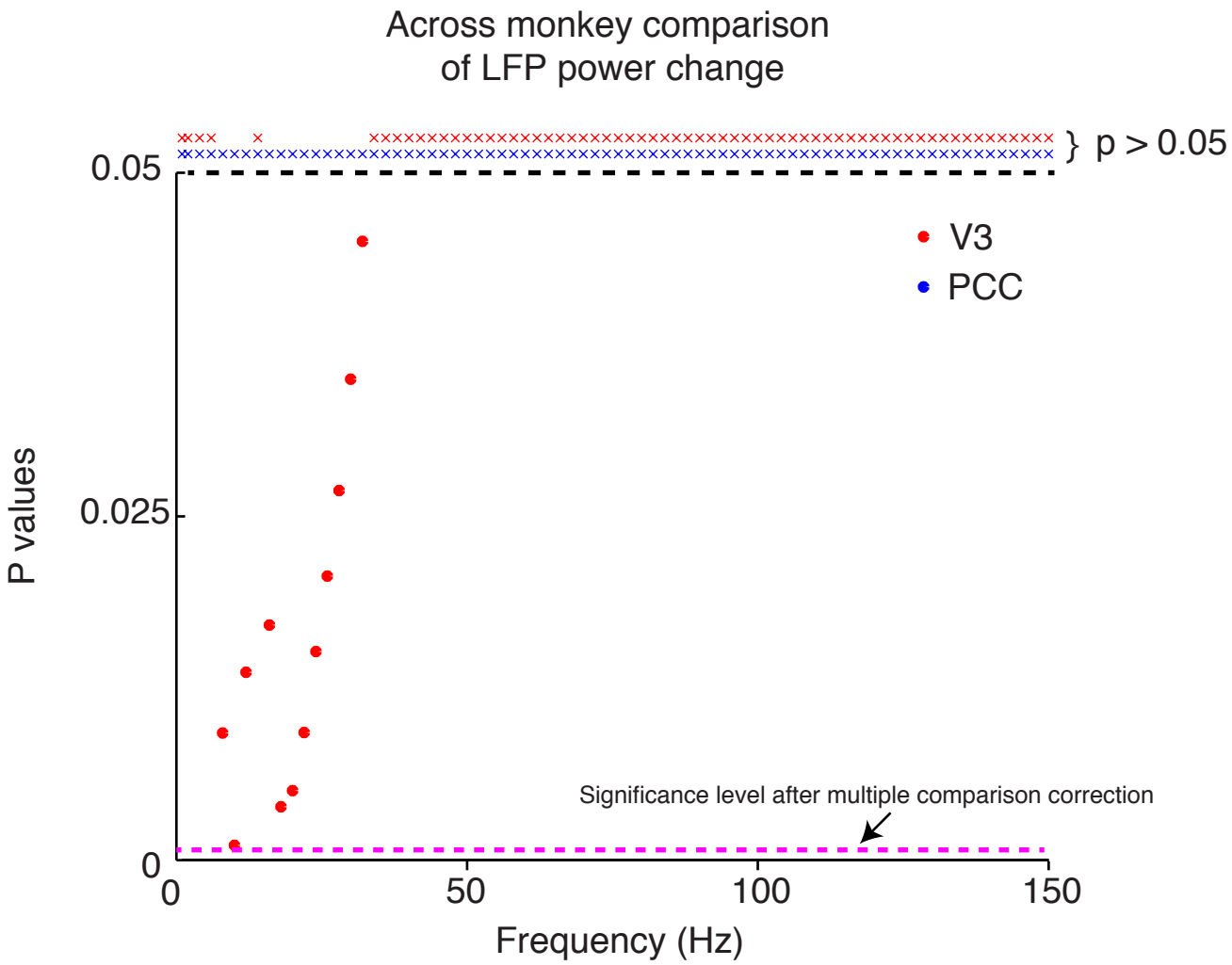

Figure S5. The p values (without multiple comparison correction) for the across monkey comparison of modulation in LFP power at each frequency. LFP power modulation is computed the same as in Figure 2B (5-15 s after the onset of visual stimulation relative to the subsequent 30 s of darkness). P values larger than 0.05 are shown as crosses. In PCC, there is no significant difference in power between the two monkeys at any frequency. In V3, there is no significant difference except at 8-32 Hz, where the LFP power modulation for Monkey 1 is less than that of Monkey 2. Even this difference is not significant if corrected for multiple comparisons (criterion level of P = 0.05/76, dashed magenta line).

Supplementary Figure S6

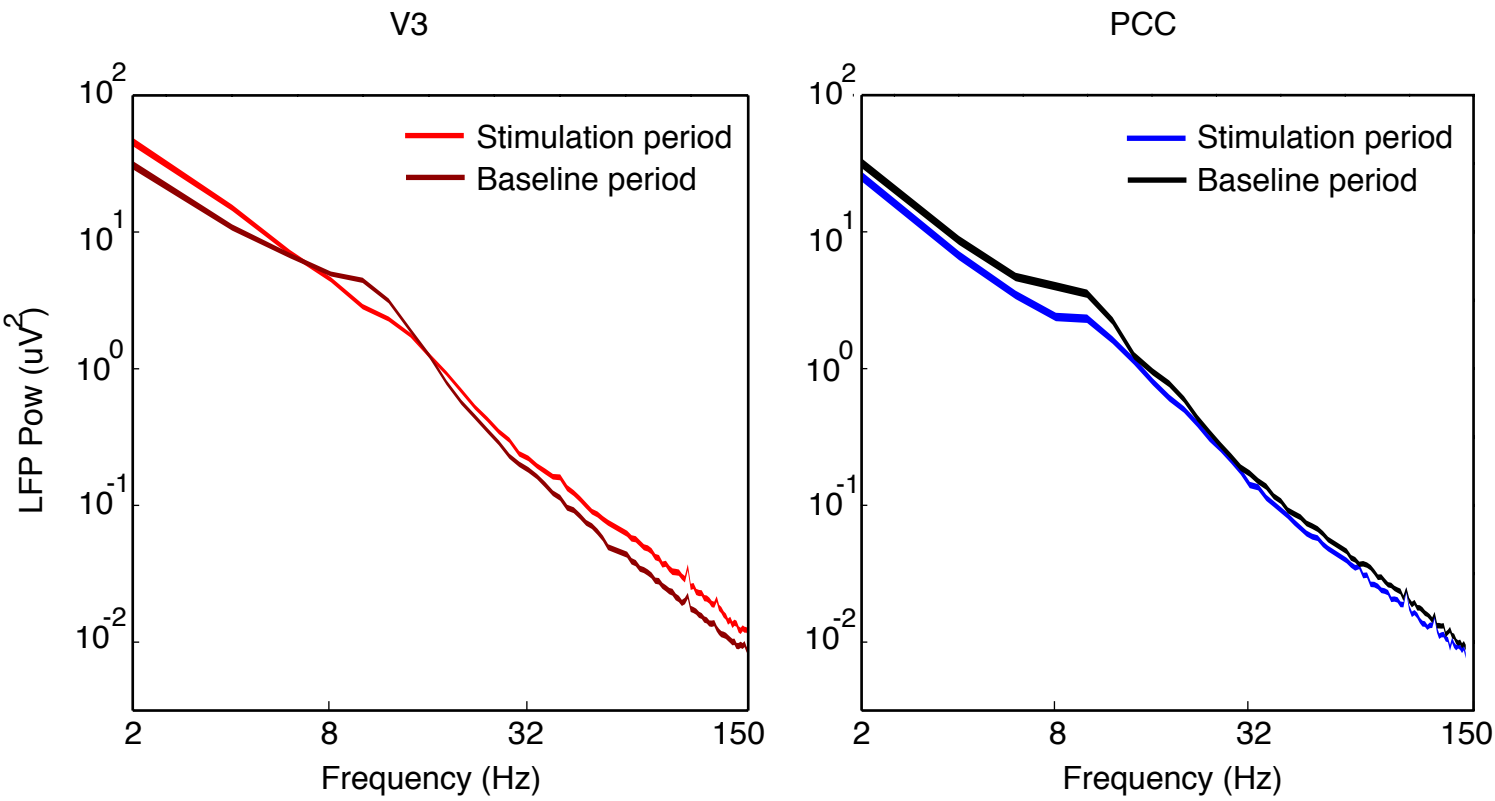

Figure S6. LFP power (mean ± SEM) as a function of frequency (log) during stimulation for V3 and PCC for the visual stimulation period and the baseline period (0-5 s before stimulus onset). Overall, LFP power is inversely proportional to the frequency. In V3, LFP power increases during stimulation compared to the baseline, expect for (6-16 Hz). In PCC, LFP power decreases during stimulation compared to the baseline.

Supplementary Figure S7

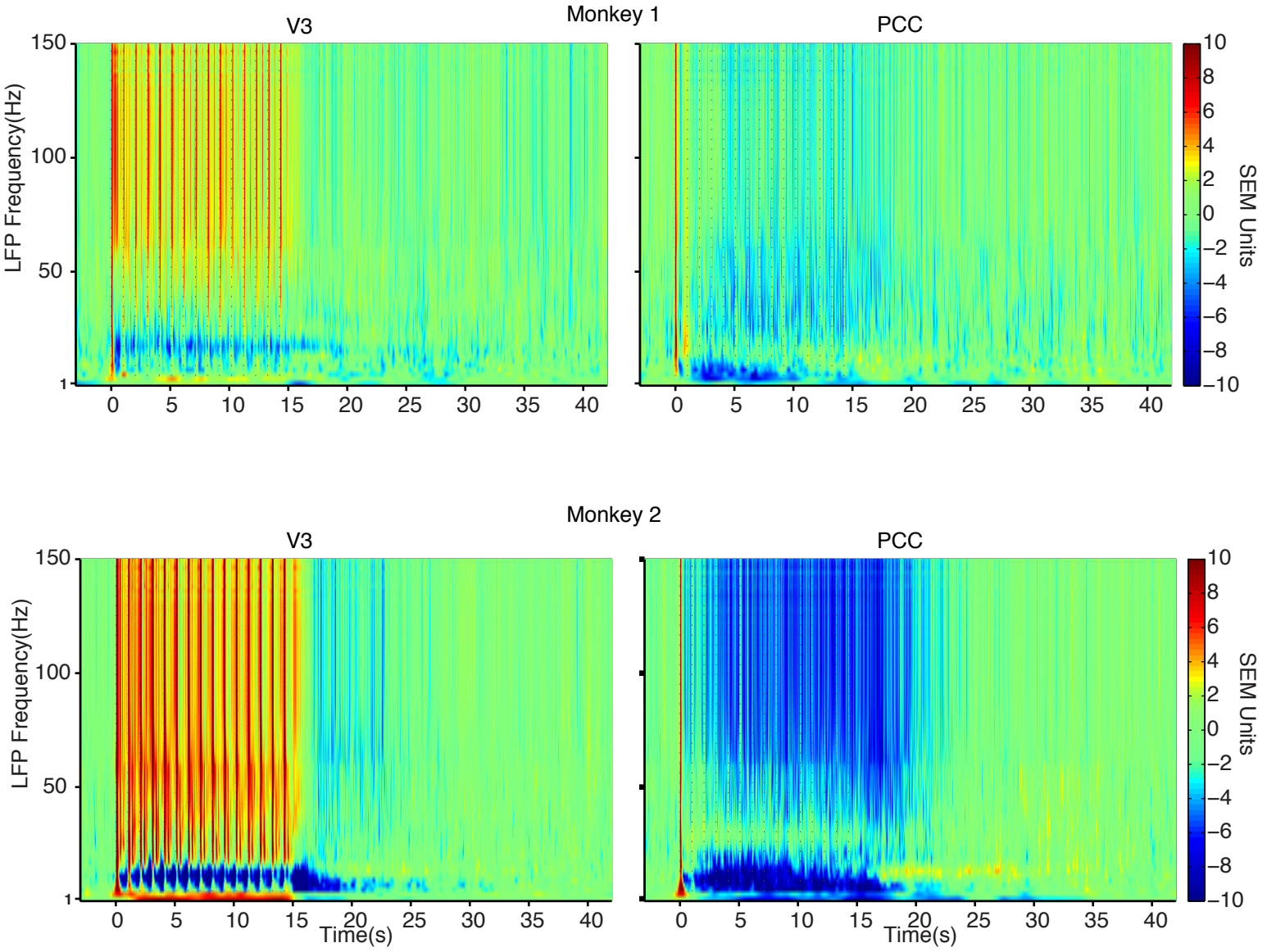

Figure S7. LFP power modulation relative to baseline (0-5 s before stimulus onset) in standard error units (SEM is estimated based on baseline activity) for both monkeys.

Supplementary Figure S8

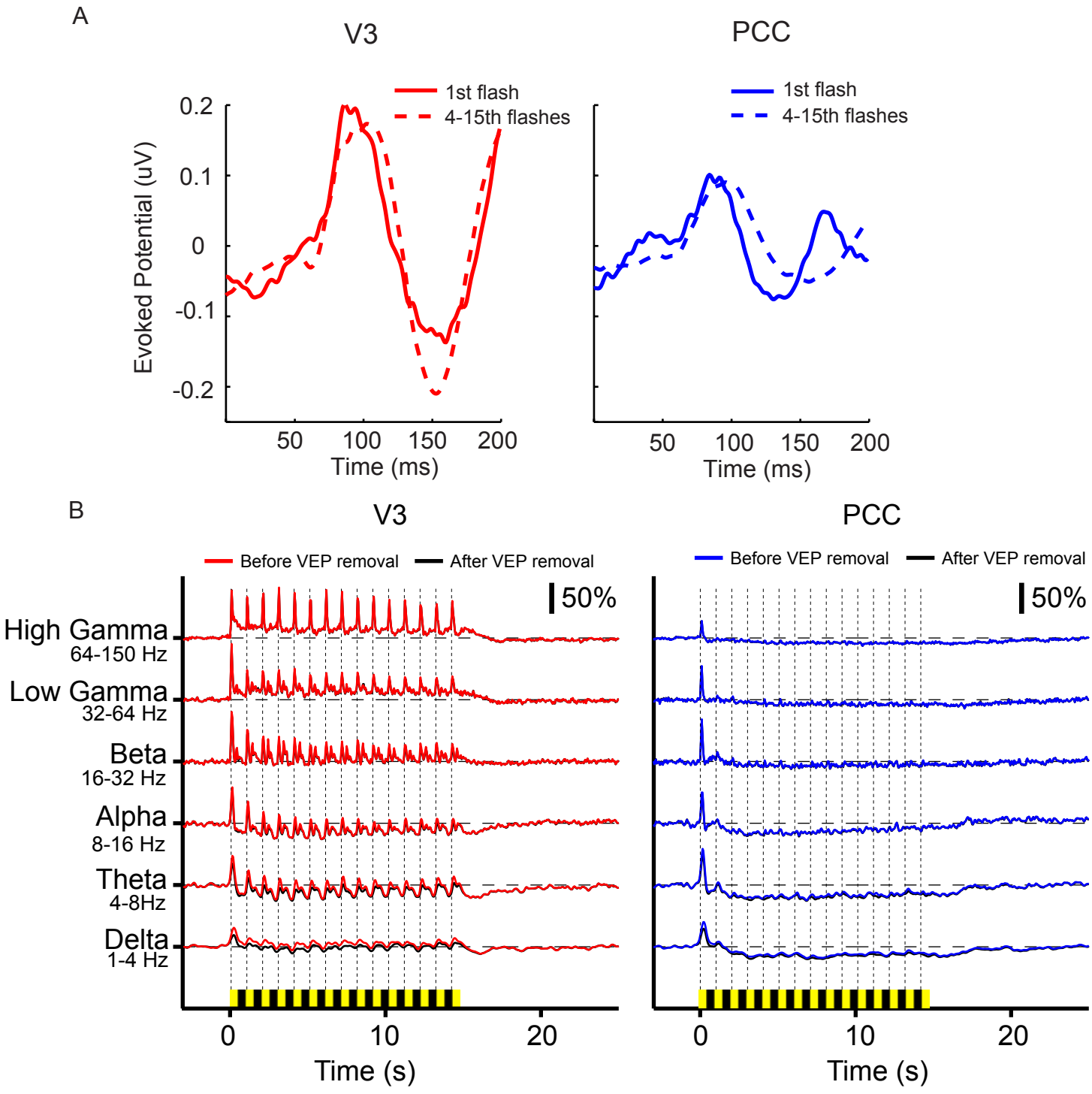

Figure S8. A. Visual stimulus evoked potential (VEP) for V3 and PCC. The positive component around 100 ms could correspond to the P100, and the negative component around 150 ms in V3 could correspond to the N140. VEPs associated with the stimulus onset (solid lines, first flash) are similar to those evoked by the later flashes (dashed lines, 4-15th flashes). This is different from oxygen responses, which show a prominent transient response to the stimulus onset and a sustained response (positive in V3 and negative in PCC) to later flashes. B. Percent modulation of LFP power for standard EEG bands before and after removing VEP. Removal of VEP slightly decreased LFP responses for both transient and sustained components, but the decrease is so small that the data before (colored) and after (black) VEP removal are almost indistinguishable.

Supplementary Figure S9

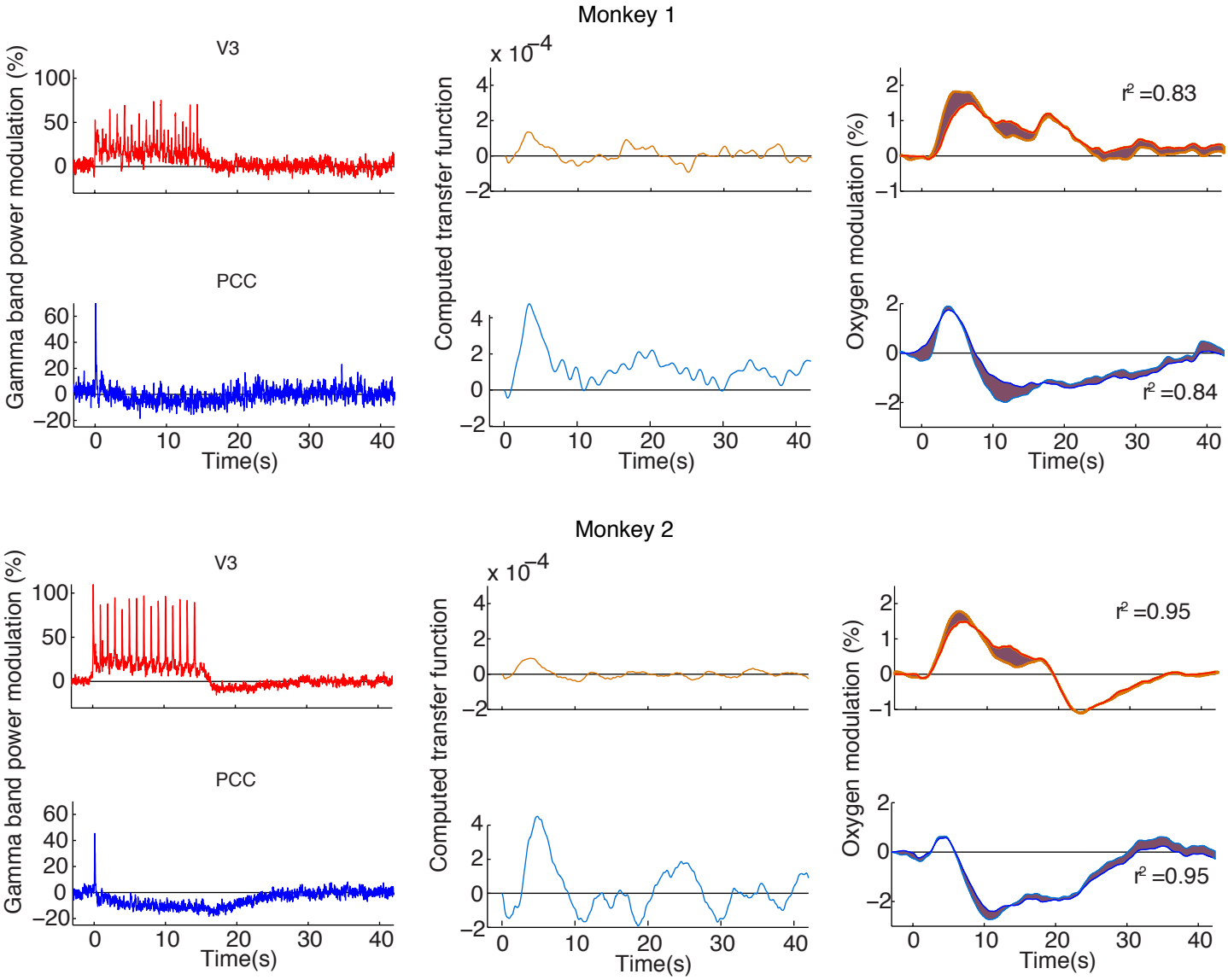

Figure S9. A computed transfer function (see text) does well in both areas but is smaller in V3 (orange in the second column) and contains an initial negativity only in PCC (cyan in the second column) for both monkeys.

Supplementary Figure S10

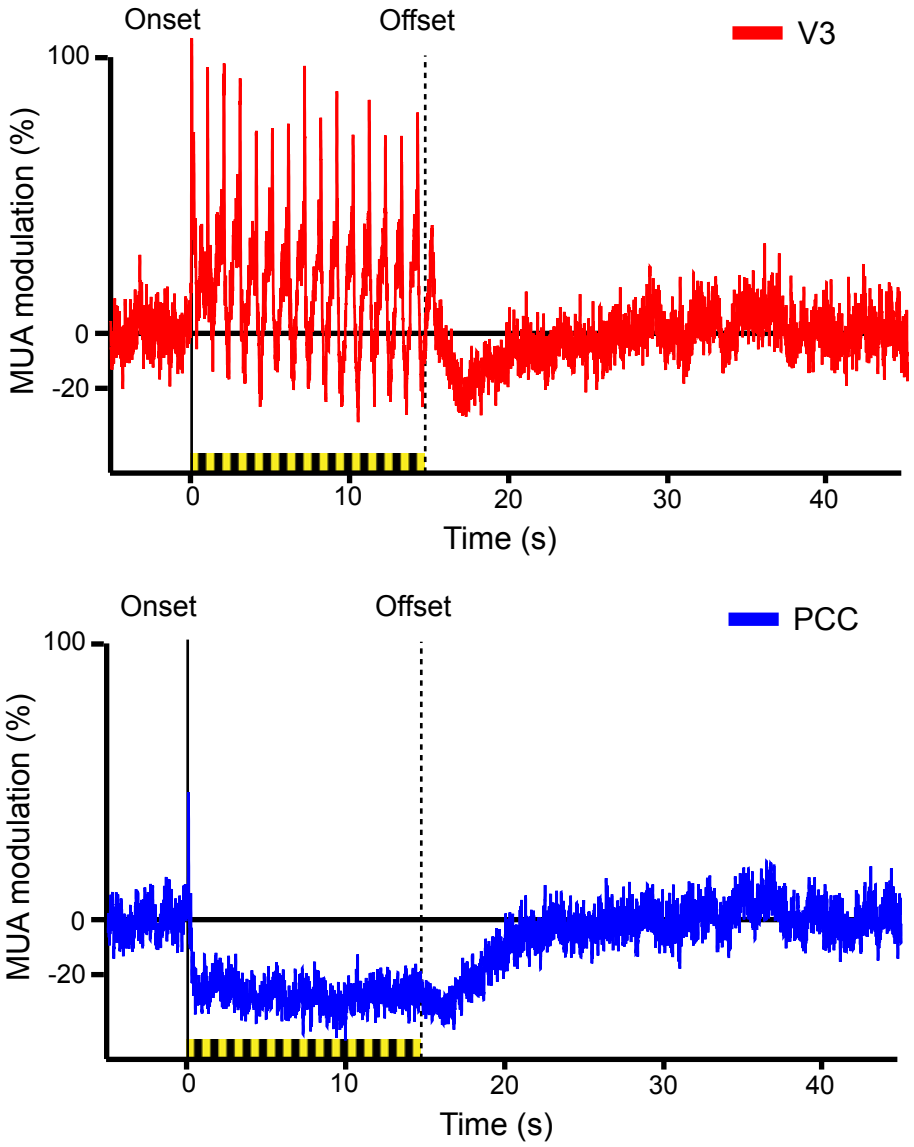

Figure S10. Percent multiple-unit activity (MUA) modulation relative to the period 0-5 s before stimulus onset. Yellow-black bars mark the 15 s, 1 Hz stroboscopic flashing stimulus. Electrophysiological signals were band-pass filtered (800Hz to 8kHz) and events exceeding 2.5 times the root mean square of the filtered signal were considered as MUA events. V3 shows complex phasic responses riding on top of a tonic increase in MUA activity relative to baseline. PCC shows smaller phasic responses at the onset of the first flash followed by a tonic decrease. Data from 397 trials in V3 and 398 in PCC from one monkey are included.